Insulin-promoted mobilization of GLUT4 from a perinuclear storage site requires RAB10

Alexandria Brumfield[a], Natasha Chaudhary[a,†], Dorothee Molle[a], Jennifer Wen[a], Johannes Graumann[b,‡], and Timothy E. McGraw[a,c,*]

[a]Department of Biochemistry and [c]Department of Cardiothoracic Surgery, Weill Cornell Medical College, New York, NY 10065; [b]Weill Cornell Medical College in Qatar, Education City, 24144 Doha, State of Qatar

ABSTRACT **Insulin controls glucose uptake into muscle and fat cells by inducing a net redistribution of glucose transporter 4 (GLUT4) from intracellular storage to the plasma membrane (PM). The TBC1D4-RAB10 signaling module is required for insulin-stimulated GLUT4 translocation to the PM, although where it intersects GLUT4 traffic was unknown. Here we demonstrate that TBC1D4-RAB10 functions to control GLUT4 mobilization from a *trans*-Golgi network (TGN) storage compartment, establishing that insulin, in addition to regulating the PM proximal effects of GLUT4-containing vesicles docking to and fusion with the PM, also directly regulates the behavior of GLUT4 deeper within the cell. We also show that GLUT4 is retained in an element/domain of the TGN from which newly synthesized lysosomal proteins are targeted to the late endosomes and the ATP7A copper transporter is translocated to the PM by elevated copper. Insulin does not mobilize ATP7A nor does copper mobilize GLUT4, and RAB10 is not required for copper-elicited ATP7A mobilization. Consequently, GLUT4 intracellular sequestration and mobilization by insulin is achieved, in part, through utilizing a region of the TGN devoted to specialized cargo transport in general rather than being specific for GLUT4. Our results define the GLUT4-containing region of the TGN as a sorting and storage site from which different cargo are mobilized by distinct signals through unique molecular machinery.**

Monitoring Editor
Adam Linstedt
Carnegie Mellon University

Received: Jun 4, 2020
Revised: Oct 30, 2020
Accepted: Nov 4, 2020

INTRODUCTION

Regulation of glucose uptake by fat and muscle cells, essential for the maintenance of whole-body glucose homeostasis, is determined by the levels of glucose transporter 4 (GLUT4) in the plasma membranes (PM) of these cells (Klip *et al.*, 2019). GLUT4 cycles between intracellular compartments and the PM, with the distribution determined by the rates of exocytosis and endocytosis (Martin *et al.*, 2000a, 2006; Foster *et al.*, 2001; Karylowski *et al.*, 2004). The main effect of insulin is to stimulate GLUT4 exocytosis to increase the amount of PM GLUT4, thereby promoting increased glucose uptake (Klip *et al.*, 2019).

This article was published online ahead of print in MBoC in Press (http://www.molbiolcell.org/cgi/doi/10.1091/mbc.E20-06-0356) on November 11, 2020.

This article was published online ahead of print in *MBoC in Press* (https://doi.org/10.1091/mbc.E20-06-0356) on 1 January 2021 and in bioRxiv (https://www.biorxiv.org/content/10.1101/2020.04.14.040683v1) https://doi.org/10.1101/2020.04.14.040683

Conflict of interest: The authors declare that the work was performed in the absence of any financial relationships that could be construed as a potential conflict of interest.

Author contributions: A.B., N.C., D.M., and J.W. designed, performed, and analyzed experiments; J.G. performed mass spectrometry; A.B. and T.E.M. wrote the manuscript; T.E.M. conceived of the project, designed and analyzed experiments, and supervised the project.

Present addresses: †Lunenfeld-Tanenbaum Research Institute, Mount Sinai Hospital, Toronto, Ontario M5G 1X5, Canada; ‡Biomolecular Mass Spectrometry, Max Planck Institute for Heart and Lung Research, 61231 Bad Nauheim, Germany, and The German Center for Cardiovascular Research (DZHK), Partner Site Rhine-Main, Max Planck Institute for Heart and Lung Research, 61231 Bad Nauheim, Germany.

*Address correspondence to: Timothy E. McGraw (temcgraw@med.cornell.edu).

Abbreviations used: ARG, arginine; ATP7A, Menkes copper-transporting ATPase; BCS, bathocuproinedisulfonic acid disodium salt; BFP, blue fluorescent protein; CHC, clathrin heavy chain; ER, endoplasmic reticulum; ERES, endoplasmic reticulum exit site; ERGIC, ER-to-Golgi intermediate compartments; GAP, GTPase-activating protein; GLUT4, glucose transporter 4; HA, hemagglutinin; IF, immunofluorescence; IRV, insulin-responsive vesicle; KIF13, Kinesin 13; LRRK2, leucine-rich repeat kinase 2; LYS, lysine; MPR, mannose 6-phosphate receptor; PBS, phosphate-buffered saline; PD, Parkinson's disease; PM, plasma membrane; SILAC, stable isotope labeling with amino acids in culture; STX6, Syntaxin6; TGN, *trans*-Golgi network; TGN46, *trans*-Golgi Network Protein 2; TR, transferrin receptor; WT, wild type.

In the basal state (unstimulated cells), the majority of GLUT4 resides intracellularly in perinuclear compartments that are in part *trans*-Golgi network (TGN) in nature (Shewan *et al.*, 2003; Li *et al.*, 2009; Foley and Klip, 2014) and in specialized vesicles (referred to as insulin-responsive vesicles, IRVs) dispersed throughout the cytosol (Xu and Kandror, 2002; Larance *et al.*, 2005; Jedrychowski *et al.*, 2010), whose delivery to the PM is regulated by insulin (Karylowski *et al.*, 2004). GLUT4 in the PM cycles back to the TGN via the endosomal pathway (Lampson *et al.*, 2001; Karylowski *et al.*, 2004; Chen *et al.*, 2012). Targeting GLUT4 from endosomes to the TGN has an important role in basal intracellular GLUT4 retention. Mutations in GLUT4 that disrupt its traffic from endosomes to the TGN are poorly retained in basal conditions and are not properly translocated to the PM on insulin stimulation (Piper *et al.*, 1993; Shewan *et al.*, 2003; Govers *et al.*, 2004; Blot and McGraw, 2008a). These results identify the TGN as the site for formation of IRVs. The TGN is a main sorting compartment along the biosynthetic and endocytic pathways. Cargoes to be targeted to distinct destinations are sorted and packaged into the correct transport vesicles in the TGN. The relationship between the TGN containing GLUT4 and the TGN involved in the traffic of other cargoes is not known (Lampson *et al.*, 2001; Shewan *et al.*, 2003; Karylowski *et al.*, 2004; Foley and Klip, 2014).

Insulin signaling triggers multiple discrete molecular events that mediate efficient recruitment, docking, and fusion of IRVs with the PM (Gonzalez and McGraw, 2006; Bai *et al.*, 2007; Xiong *et al.*, 2010). These events lead to a decrease in the size of the intracellular GLUT4 pool concomitant with an increase of GLUT4 in the PM. As GLUT4 in the PM is in equilibrium with intracellular GLUT4, endocytosis of GLUT4 dynamically removes GLUT4 from the PM. Thus, maintenance of the insulin-stimulated dynamic increase in GLUT4 in the PM requires the continual ferrying of GLUT4-containing IRVs to the PM. Insulin signaling can add to the IRV pool by increasing the rate of GLUT4 mobilization from the TGN in nascent IRVs. Despite the biological importance, insulin regulation of GLUT4 trafficking at the perinuclear region has not been thoroughly interrogated.

A key aspect of insulin regulation of GLUT4 trafficking is inhibition of the GTPase-activating protein (GAP) TBC1D4/AS160 (Sano *et al.*, 2003; Eguez *et al.*, 2005), allowing for activation of its target RAB, RAB10 (Sano *et al.*, 2007). In 3T3-L1 adipocytes and primary adipocytes, knockdown of TBC1D4 releases the inhibition of GLUT4 exocytosis in the basal state by 50% (Eguez *et al.*, 2005; Lansey *et al.*, 2012), and depletion of RAB10 in cultured and primary adipocytes specifically blunts insulin-stimulated GLUT4 translocation by 50% (Sano *et al.*, 2007; Sadacca *et al.*, 2013; Vazirani *et al.*, 2016). These data demonstrate insulin-stimulated GLUT4 exocytosis is regulated by both TBC1D4-RAB10-dependent and -independent mechanisms. Overexpressed RAB10 has been shown to reside on IRVs in adipocytes (Chen *et al.*, 2012), and total internal reflection fluorescence (TIRF) microscopy studies have demonstrated RAB10 functions at a step prior to IRV fusion with the PM (Sadacca *et al.*, 2013). Thus, it is commonly thought RAB10 regulates IRV recruitment and/or docking with the PM. In other cell types, RAB10 is required for regulated trafficking processes that involve vesicle delivery to the PM (Babbey *et al.*, 2010; Wang *et al.*, 2010; Liu *et al.*, 2013; Isabella and Horne-Badovinac, 2016; Etoh and Fukuda, 2019), and RAB10 has been shown to localize to both perinuclear and vesicular compartments (Wang *et al.*, 2010; Liu *et al.*, 2013).

We have previously identified SEC16A as a novel RAB10-interacting protein required for insulin-stimulated GLUT4 translocation (Bruno *et al.*, 2016). Knockdown of SEC16A in 3T3-L1 adipocytes specifically blunts insulin-stimulated GLUT4 translocation by 50%, with no additivity of double knockdown of RAB10 and SEC16A (Bruno *et al.*, 2016). Interestingly, a pool of SEC16A localizes to structures in the perinuclear region that encircle GLUT4-containing perinuclear membranes (Bruno *et al.*, 2016). SEC16A is known to localize to endoplasmic reticulum exit sites (ERES) and act as a scaffold for the organization of COPII components required for the budding of COPII vesicles (Whittle and Schwartz, 2010; Sprangers and Rabouille, 2015). In adipocytes, SEC16A's role in GLUT4 trafficking is independent of its role in ERES function since knockdown of other components of the ER exit site machinery, which blunt secretion, is without effect on GLUT4 translocation (Bruno *et al.*, 2016). SEC16A's perinuclear localization (Bruno *et al.*, 2016) suggests the RAB10-SEC16A module might function at the perinuclear region to regulate IRV formation. RAB10 then rides along newly formed IRVs (Chen *et al.*, 2012), while the lack of SEC16A localization to IRVs (Bruno *et al.*, 2016) demonstrates that SEC16A does not. In this study, we use a novel proteomic approach to demonstrate that GLUT4 resides in a region of the TGN where specialized cargoes are sorted and mobilized by specific stimuli and, using a novel live-cell imaging assay, we demonstrate that insulin promotes the mobilization of GLUT4 from the TGN through RAB10 activity.

RESULTS

GLUT4 is retained in a region of the TGN from which specialized cargoes are sorted and mobilized

The first approach we took to gain insight into GLUT4 trafficking at the perinuclear region was to identify proteins that reside with GLUT4 in the perinuclear compartment of 3T3-L1 adipocytes. It has previously been shown that mutation of the phenylalanine of the GLUT4 amino terminal F^5QQI motif (amino acid positions 5 through 8) to a tyrosine (Y^5QQI) redistributes GLUT4 to the TGN perinuclear compartment from cytosolic puncta (Blot and McGraw, 2008a). HA-GLUT4-GFP is a reporter extensively used in studies of GLUT4 traffic (Blot and McGraw, 2008b). HA-GLUT4-GFP with a F^5QQI to Y^5QQI mutation (F^5Y-HA-GLUT4-GFP) displays enhanced intracellular retention in the TGN and concentration around the nucleus (Figure 1A), as demonstrated by increased overlap with TGN markers Syntaxin6 (STX6) and *trans*-Golgi Network Protein 2 (TGN46) (Figure 1, A–C). F^5Y-GLUT4 continually cycles to and from the PM, and thus is dynamically concentrated in the TGN (Blot and McGraw, 2008a). GLUT4 in which an alanine is substituted for phenylalanine in the F^5QQI motif (F^5A-GLUT4) is not as efficiently targeted to the TGN as compared with wild-type (WT) GLUT4 (Piper *et al.*, 1993; Govers *et al.*, 2004; Blot and McGraw, 2008a). Consequently, F^5A-HA-GLUT4-GFP was predominantly localized in vesicular elements throughout the cytoplasm and was not well concentrated around the nucleus (Figure 1A), as indicated by the decreased overlap with STX6 and TGN46 (Figure 1, A–C). Given that F^5Y-GLUT4 is enriched in the TGN as compared with both WT GLUT4 and F^5A-GLUT4 (Blot and McGraw, 2008a), we reasoned that proteins colocalized with GLUT4 in the TGN (the same TGN membrane as GLUT4) would be enriched in a detergent-free immunoabsorption of F^5Y-GLUT4 because membrane integrity is preserved in this protocol. Membrane compartments containing HA-GLUT4-GFP were isolated by detergent-free immunoabsorption with anti-GFP-antibody from mechanically disrupted unstimulated 3T3-L1 adipocytes stably expressing HA-GLUT4-GFP, F^5Y-HA-GLUT4-GFP or F^5A-GLUT4-GFP. We used stable isotope labeling with amino acids in culture (SILAC) to quantitatively compare by mass spectrometry proteins coimmunoabsorbed with these different GLUT4 constructs (Ong *et al.*, 2002; Ibarrola *et al.*, 2003). Pairwise comparisons of WT versus F^5Y and F^5A versus F^5Y were performed in duplicate inverting which cells were grown in the heavy amino acid medium, generating four

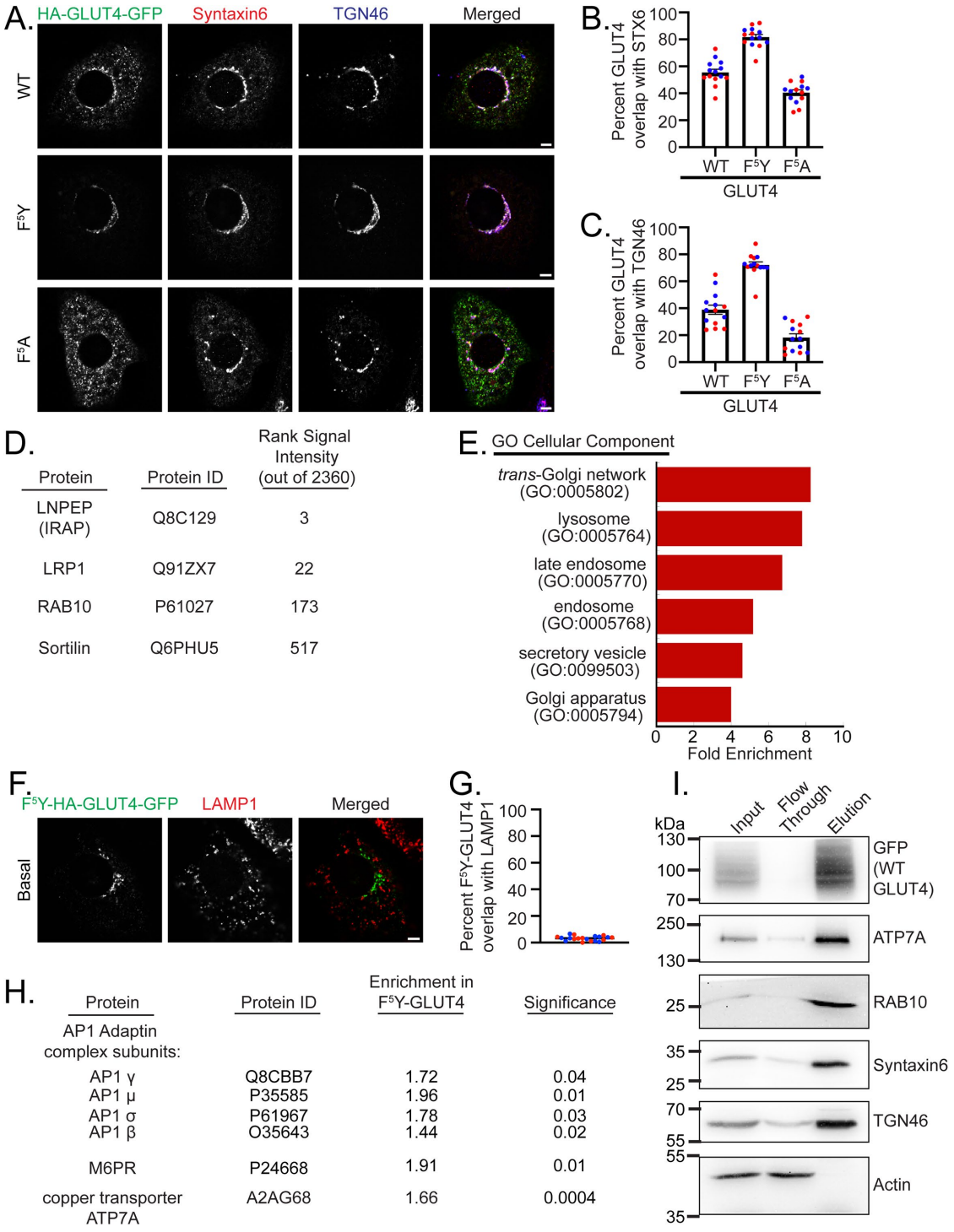

FIGURE 1: Proteomic analysis of GLUT4-containing perinuclear compartments. (A) Representative Airyscan confocal single plane images of cells expressing WT, F^{5}Y-, or F^{5}A-HA-GLUT4-GFP and labeled for STX6 and TGN46 by IF. (B) Quantification of percent overlap of WT, F^{5}Y, and F^{5}A GLUT4 with STX6. Individual cells ± SEM from $N = 2$ assays. Cells color coded by experiment. (C) Quantification of percent overlap of WT, F^{5}Y, and F^{5}A GLUT4 with TGN46. Individual cells ± SEM from $N = 2$ assays. Cells color coded by experiment. (D) Proteins identified in immunoabsorption experiments that are known to colocalize with GLUT4, rank based on summed signal intensity from four immunoabsorption experiments. (E) Panther Gene Ontology (GO) cellular component analysis for localization of proteins increased in F^{5}Y-GLUT4 compartments immunoabsorption. (F) Representative Airyscan confocal single plane images of cells expressing F^{5}Y-HA-GLUT4-GFP mutant and labeled for LAMP1 by IF. (G) Quantification of percent overlap of F^{5}Y GLUT4 with LAMP1. Individual cells ± SEM from $N = 2$ assays. Cells color coded by experiment. (H) Fold increase of AP1 adaptin complex subunits, MPR, and copper transporter ATP7A in F^{5}Y-GLUT4 compartments immunoabsorption. (I) Representative Western blots of immunoabsorbed WT HA-GLUT4-GFP compartments using anti-GFP beads. Elution contains proteins coimmunoabsorbed with GLUT4 compartments; flow-through contains proteins not coimmunoabsorbed. Bars, 5 μm.

different data sets of proteins immunoabsorbed with F5Y compared with WT (two sets) and compared with F5A (two sets).

There were 2360 proteins in the merged data from the four sets of data. The experimental premise that mechanical disruption preserves, at least partially, the integrity of membrane compartments/domains was validated by the fact that relative abundance (summed signal intensity) of proteins previously identified to colocalize but not directly interact with GLUT4, including LNPEP (or IRAP; Garza and Birnbaum, 2000), LRP1 (Jedrychowski *et al.*, 2010), RAB10 (Sano *et al.*, 2007; Chen *et al.*, 2012), and Sortilin (Morris *et al.*, 1998), was in the top 20% of proteins ranked based on signal intensity (Figure 1D and Supplemental Table S1). Of note, LNPEP, which is known to traffic via the same pathway as GLUT4 (Garza and Birnbaum, 2000) and is therefore expected to be efficiently coimmunoabsorbed with GLUT4, was the third most abundant protein in the immunoabsorption based on signal intensity.

The aim of this study was to identify proteins enriched in the F5Y-GLUT4 immunoabsorption; therefore, we focused our analyses on the set of 508 proteins that in the pooled data set were increased in the F5Y-GLUT4 immunoabsorption by greater than 1.3-fold by SILAC ratio (Supplemental Table S2). Gene ontology cellular component analyses (Ashburner *et al.*, 2000; Consortium, 2019) revealed a significant enrichment for proteins annotated to be localized to the TGN and TGN transport vesicles, including STX6 and TGN46 (Figure 1E). In addition, there was enrichment of Golgi, endosome, exocytic vesicles, and the ER-to-Golgi intermediate compartment proteins (Figure 1E), consistent with GLUT4 being dynamically distributed among a number of intracellular compartments (Karylowski *et al.*, 2004).

Unexpectedly, there was also a significant enrichment of late endosome and lysosome proteins (Figure 1E). This enrichment was not because F5Y-GLUT4 is localized to late endosomes/lysosomes as there was no significant overlap between F5Y-GLUT4 and LAMP1 (Figure 1, F and G). The majority of newly synthesized lysosomal proteins are delivered to the lysosomes by a pathway involving targeting from the TGN to the late endosomes (Braulke and Bonifacino, 2009). Soluble lysosome proteins, which are modified by mannose 6-phosphate in the ER, are diverted from delivery to the PM at the level of the TGN via a mechanism requiring the mannose 6-phosphate receptor (MPR) and the AP1 clathrin adaptin complex (Braulke and Bonifacino, 2009). Thus, an explanation for the enrichment of F5Y-GLUT4 with lysosomal proteins is that the GLUT4-containing perinuclear concentration is a specialized subcompartment of the TGN where lysosomal proteins are diverted from delivery to the PM by sorting to specialized transport vesicles. In support of that hypothesis, the MPR and the four subunits of the AP1 complex (AP1 μ, σ, β, γ), components of the machinery that targets lysosomal proteins to the late endosomes, were significantly enriched in the F5Y-GLUT4 immunoabsorption (Figure 1H). Based on these data, we propose that the region of the TGN enriched for F5Y-GLUT4 is involved in the sorting of cargoes that exit the TGN via specialized vesicles, diverting cargo from nonspecialized vesicles that mediate constitutive traffic to the PM.

The immunoabsorption data identified the Menkes copper transporter, ATP7A, as enriched in the F5Y-GLUT4-containing perinuclear compartments (Figure 1H). We confirm by Western blotting that ATP7A is enriched in immunoabsorbed GLUT4-containing membranes, as is RAB10, STX6, and TGN46 (Figure 1I). Previous studies have also identified that ATP7A coimmunoabsorbs with GLUT4 (Larance *et al.*, 2005). ATP7A, which is expressed in a broad variety of cell types, has a role in protecting cells against copper overload. At physiological copper levels, ATP7A primarily localizes to the TGN, but with an increased copper load, ATP7A translocates to the PM, where it pumps copper from cells (Petris *et al.*, 1996). In low copper conditions, achieved by treatment with copper chelator bathocuproinedisulfonic acid disodium salt (BCS), ATP7A was largely colocalized with GLUT4 in the TGN of 3T3-L1 adipocytes, validating the mass spectrometry data (Figure 2, A and B). Challenging cells with elevated copper resulted in a decrease in the intensity of ATP7A in the STX6-postive TGN and an increase in ATP7A labeling in cytosolic vesicles (Figure 2A). Copper mobilization of ATP7A was reflected by a significant decrease in ATP7A overlap with STX6 (Figure 2C). Insulin stimulation in adipocytes results in translocation of GLUT4 to the PM, as measured by ratiometric analyses of the HA-GLUT4-GFP reporter (Figure 2D). Insulin stimulation did not affect ATP7A colocalization with STX6 (Figure 2, A and C), nor did elevated copper promote GLUT4 translocation to the PM (Figure 2, A and D). Thus, despite the high degree of colocalization of ATP7A and GLUT4, their mobilizations from the TGN are linked to distinct stimuli. Supporting this conclusion, dual stimulation with insulin and copper did not result in additive effects on mobilization of ATP7A from the STX6-positive TGN (Figure 2C) or GLUT4 translocation to the PM (Figure 2D). Given RAB10 is one of the best described molecular machinery required for insulin-stimulated GLUT4 translocation in adipocytes (Sano *et al.*, 2007), we looked to see if RAB10 is required for copper-stimulated mobilization of ATP7A from the perinuclear region. Under conditions of RAB10 knockdown, copper promoted the mobilization of ATP7A from the STX6-labeled TGN (Figure 2E) to the same degree as in WT cells (Figure 2C). Together, these data support the hypothesis that the GLUT4-containing TGN compartment is a retention and sorting hub where various stimuli mobilize specific cargo through distinct machinery.

Insulin increases the rate of GLUT4 mobilization from the perinuclear region

We next sought to demonstrate that insulin stimulation promotes the mobilization of GLUT4 from the perinuclear region of 3T3-L1 adipocytes, similar to copper stimulation promoting the mobilization of ATP7A. With insulin stimulation it was visually apparent that the GLUT4-containing IRV pool was decreased in size concomitant with an increase in GLUT4 in the PM (Figure 3A). However, in static images, an effect of insulin on GLUT4 in the TGN was not apparent. Visualizing the mobilization of GLUT4 from the perinuclear compartment in live-cell imaging would prove very useful in determining if insulin regulates GLUT4 trafficking at the perinuclear region yet has been confounded by the difficulty of distinguishing GLUT4-containing vesicles that have budded from the perinuclear compartments from those that have been endocytosed at the PM. To overcome this limitation, we tagged GLUT4 with an irreversible green-to-red photoconvertible protein mEos3.2 (Zhang *et al.*, 2012) (HA-GLUT4-mEos3.2) and visualized the mobilization of HA-GLUT4-mEos3.2 that has been acutely photoconverted from green to red in a region of the perinuclear compartment and thus could be distinguished from the remainder of HA-GLUT4-mEos3.2 in the cell (Figure 3B). After photoconversion, the decrease over time in red HA-GLUT4-mEos3.2 intensity in the photoconverted region represents GLUT4 that has been mobilized from the perinuclear region, and the return over time of the green HA-GLUT4-mEos3.2 intensity in the photoconverted region represents GLUT4 that has been mobilized to the perinuclear region (Figure 3B). Importantly, the trafficking of HA-GLUT4-mEos3.2 was similar to the well-characterized HA-GLUT4-GFP reporter (Figure 3C). Furthermore, in fixed cells, successive image acquisition did not result in a decrease in the red HA-GLUT4-mEos3.2 intensity in the photoconverted

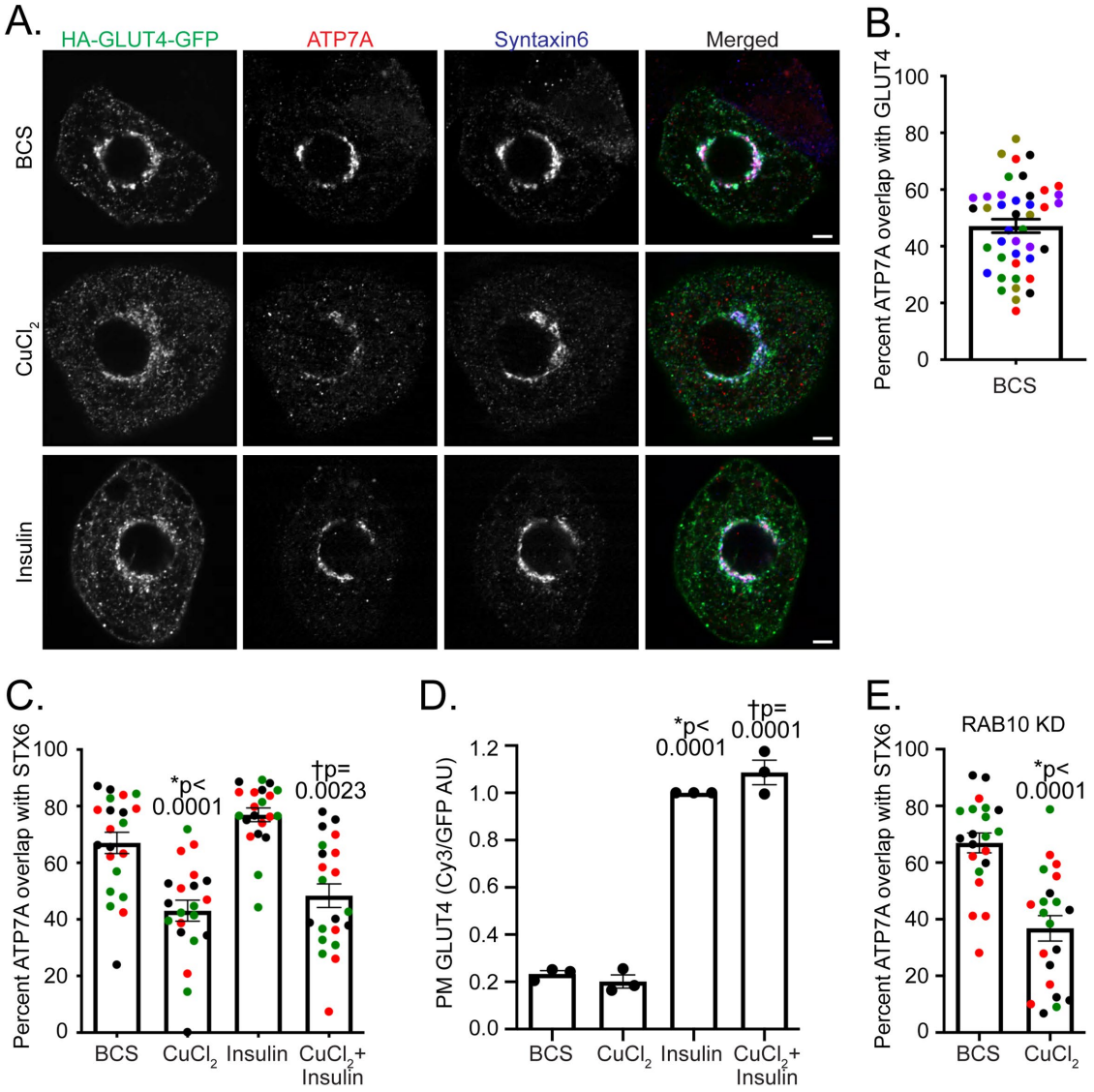

FIGURE 2: Copper, but not insulin, stimulation results in mobilization of the copper transporter ATP7A from GLUT4-containing perinuclear compartments. (A) Representative Airyscan confocal single plane images of cells expressing HA-GLUT4-GFP and labeled for native copper transporter ATP7A and STX6 by IF. Cells treated with 200 μM BCS, followed by treatment with 200 μM copper or 1 nM insulin as described in *Materials and Methods*. Bars, 5 μm. (B) Quantification of percent overlap of ATP7A with GLUT4. Individual cells ± SEM from $N = 6$ assays. Cells color coded by experiment. (C) Quantification of percent overlap of ATP7A with STX6 under BCS, copper, insulin, and dual copper and insulin-stimulated conditions. Individual cells ± SEM from $N = 3$ assays. Cells color coded by experiment. *$p < 0.0001$ comparing BCS and $CuCl_2$ conditions; †$p = 0.0023$ comparing BCS and $CuCl_2$+insulin conditions (one-way ANOVA followed by Tukey's posttest). (D) Quantification of PM to total HA-GLUT4-GFP in cells under BCS, copper, insulin, and dual copper and insulin-stimulated conditions. $N = 3$ experiments ± SEM. AU, arbitrary units. *$p < 0.0001$ comparing BCS and insulin conditions; †$p < 0.0001$ comparing BCS and $CuCl_2$+insulin conditions (one-way ANOVA followed by Tukey's posttest). (E) Quantification of percent overlap of ATP7A with STX6 under BCS and copper-stimulated conditions in cells electroporated with siRNA targeting RAB10. Individual cells ± SEM from $N = 3$ assays. Cells color coded by experiment. *$p < 0.0001$ comparing BCS and copper conditions (one-way ANOVA of conditions in C and E followed by Tukey's posttest).

region (Figure 3D). These data argue that in live-cell imaging, any decrease in red HA-GLUT4-mEso3.2 intensity observed is not a result of photobleaching with successive image acquisition.

We first determined if insulin regulates the mobilization of GLUT4 from the perinuclear compartment. Under basal conditions, red HA-GLUT4-mEos3.2 was mobilized from the photoconverted region with a rate $k = 0.033$ min^{1} (Figure 3E). Under insulin-stimulated conditions, red HA-GLUT4-mEos3.2 was mobilized from the photoconverted region with a rate $k = 0.051$ min^{1} (Figure 3E), a 1.53-fold increase compared with basal conditions. These data are the first direct evidence demonstrating that insulin signaling accelerates mobilization of GLUT4 from the perinuclear region. Insulin-stimulated GLUT4 translocation in adipocytes and muscle requires activation of AKT (Klip *et al.*, 2019). Insulin regulation of GLUT4 mobilization from the perinuclear region is downstream of AKT in 3T3-L1 adipocytes, and as compared with insulin in the presence of DMSO

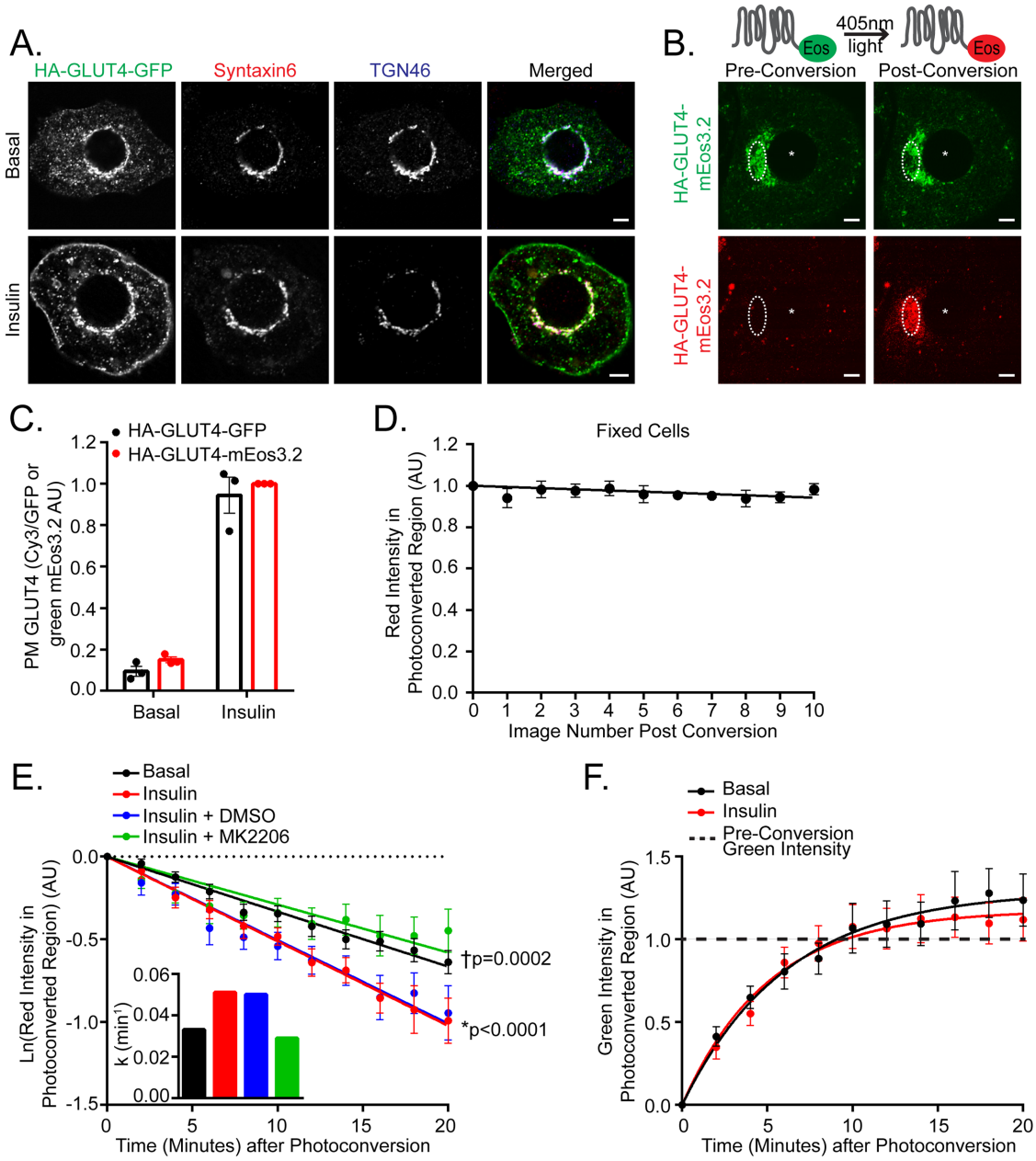

FIGURE 3: Insulin promotes mobilization of HA-GLUT4-mEos3.2 from the perinuclear region downstream of AKT. (A) Representative Airyscan confocal single plane images of basal and insulin-stimulated cells expressing HA-GLUT4-GFP and labeled for STX6 and TGN46 by IF. (B) Representative Airyscan confocal single plane images of cells expressing HA-GLUT4-mEos3.2. Green HA-GLUT4-mEos3.2 photoconverted to red HA-GLUT4-mEos3.2 in the perinuclear region (indicated by white, dashed circle) as described in *Materials and Methods*. *Nucleus. (C) Quantification of PM to total HA-GLUT4-GFP or HA-GLUT4-mEos3.2 as described in *Materials and Methods*. Serum-starved cells were stimulated with 10 nM insulin. Values were normalized to HA-GLUT4-mEos3.2 expressing, insulin condition. $N = 3$ assays ± SEM. (D) Quantification of average red HA-GLUT4-mEos3.2 intensity in the photoconverted perinuclear region of fixed cells for 10 successive images. Values were normalized to image 0. Mean normalized values ± SEM, $N = 2$ assays, 6–7 cells per assay. (E) Quantification of average red HA-GLUT4-mEos3.2 intensity in the photoconverted perinuclear region of live cells. Prior to photoconversion serum-starved cells were stimulated with 10 nM insulin, 1 μM AKT inhibitor MK2206, or equivalent volume of DMSO, where indicated, as described in *Materials and Methods*. Values were normalized to value at time 0. Mean normalized values ± SEM, $N = 5–6$ assays, 4–7 cells per assay. *$p < 0.0001$ comparing basal and insulin-stimulated slopes; †$p = 0.0002$ comparing insulin + DMSO and insulin + MK2206-stimulated slopes. Inset depicts rate of transport, determined from slope. (F) Quantification of average green HA-GLUT4-mEos3.2 intensity in the photoconverted perinuclear region of live cells. Prior to photoconversion, serum-starved cells were stimulated with 10 nM insulin where indicated. Values were normalized to value at time 0. Mean normalized values ± SEM, $N = 5–6$ assays, 4–7 cells per assay. AU, arbitrary units. Bars, 5 μm.

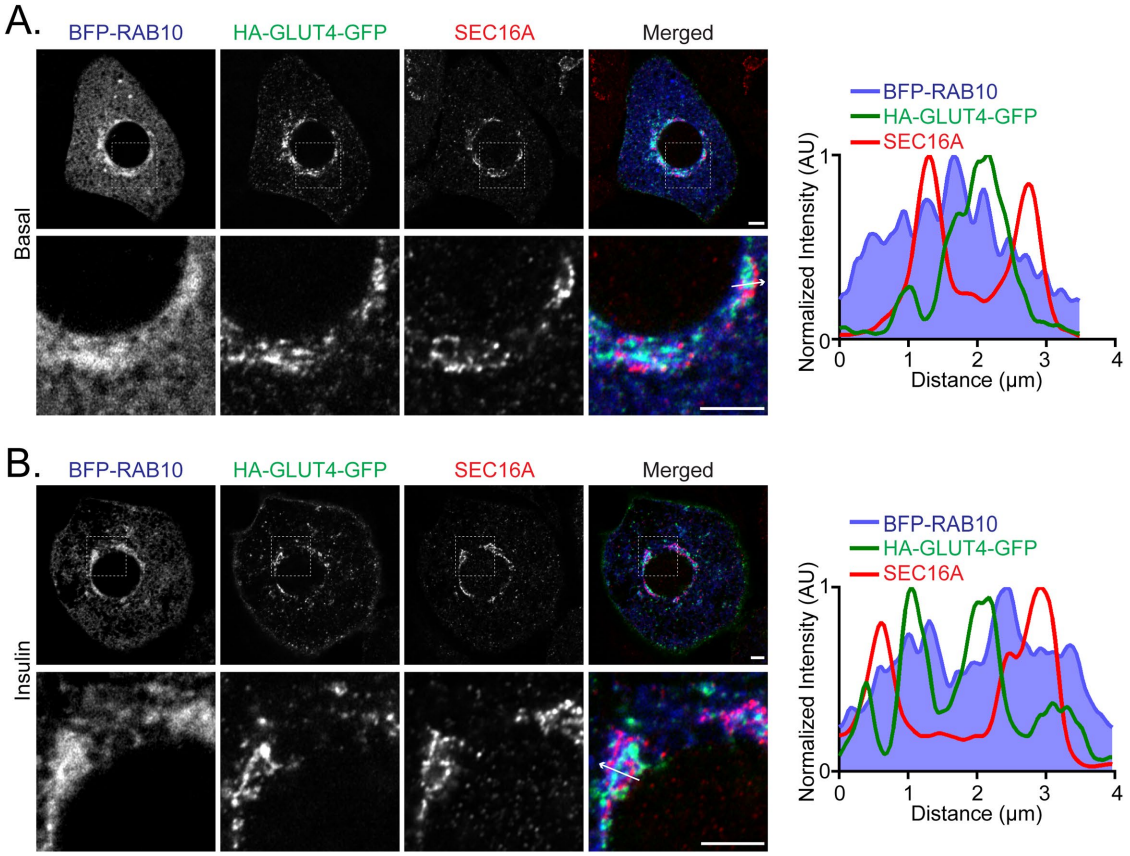

FIGURE 4: RAB10 colocalizes with HA-GLUT4-GFP and SEC16A at the perinuclear region. (A, B) Representative Airyscan confocal single plane images of (A) basal and (B) insulin-stimulated cells expressing BFP-RAB10 and HA-GLUT4-GFP and labeled for endogenous SEC16A by IF. Serum-starved cells were stimulated with 1 nM insulin. Inset (white, dashed boxed region) is displayed below. Linescan plot is BFP-RAB10, HA-GLUT4-GFP, and SEC16A fluorescence intensity along a line (indicated by white arrow). Values were normalized to each individual fluorescence maxima. Bars, 5 μm.

(vehicle), insulin in the presence of AKT inhibitor MK2206 (Tan *et al.*, 2011) could not promote the mobilization of HA-GLUT4-mEos3.2 from the perinuclear region (Figure 3E).

We next determined if insulin regulates the traffic of GLUT4 to the perinuclear region. In both basal (no stimulation) and insulin-stimulated conditions the green HA-GLUT4-mEos3.2 intensity in the photoconverted region returned to the prephotoconversion intensities with half-times of approximately 5 min (Figure 3F). Thus, GLUT4 return to the TGN is not regulated by insulin. This result, coupled with our finding that GLUT4 constitutively traffics from the TGN (Figure 3E), demonstrates that GLUT4 is dynamically concentrated in the perinuclear region.

RAB10 colocalizes with SEC16A and GLUT4 at the perinuclear region

To investigate if RAB10 contributes to insulin-stimulated mobilization of GLUT4 from the perinuclear region, we first determined the localization of RAB10 in 3T3-L1 adipocytes by expressing RAB10 tagged with blue fluorescent protein (BFP-RAB10) (Figure 4, A and B). A pool of RAB10 localized to the perinuclear region under basal and insulin-stimulated conditions, suggesting its perinuclear localization is independent of its GDP/GTP state (Figure 4, A and B). As demonstrated previously, perinuclear SEC16A-labeled structures encircled HA-GLUT4-GFP-containing perinuclear TGN membranes under basal and insulin-stimulated conditions (Bruno *et al.*, 2016) (Figure 4, A and B). Airyscan microscopy has a lateral resolution of 140 nm. Given that the width of a TGN tubule is between 500 and 1000 nm (Klumperman, 2011), the Airyscan resolution limit is enough to resolve SEC16A-labled structures encircling HA-GLUT4-GFP-containing membranes. Perinuclear BFP-RAB10 colocalized with both perinuclear SEC16A and HA-GLUT4-GFP under basal and insulin-stimulated conditions, as demonstrated by linescan analyses (Figure 4, A and B). In the context of the known functional role of RAB10 and SEC16A in GLUT4 trafficking, these data raise the possibility that RAB10 and SEC16A function at the perinuclear region to regulate GLUT4 trafficking.

The organization of RAB10-labeled, SEC16A-labeled, and GLUT4-containing perinuclear membranes is not random

The perinuclear region is compact in nature and contains a number of different membrane compartments (i.e., Golgi, ER-to-Golgi intermediate compartments (ERGIC), and ER). Thus, we sought to determine if the spatial organization of RAB10-labeled, SEC16A-labeled, and GLUT4-containing perinuclear membranes is simply due to this compact nature, or if their spatial organization is not random and is important to the function of RAB10 and SEC16A in GLUT4 trafficking. To gain insight into this question, we treated cells with nocodazole and determined if the RAB10-SEC16A-GLUT4 spatial organization is retained (Figure 5, A and C). The organization of the Golgi as a ribbon-like organelle and its perinuclear localization are highly dependent on an intact microtubule cytoskeleton (Cole *et al.*, 1996; Thyberg and Moskalewski, 1999). Nocodazole-induced disruption of microtubule

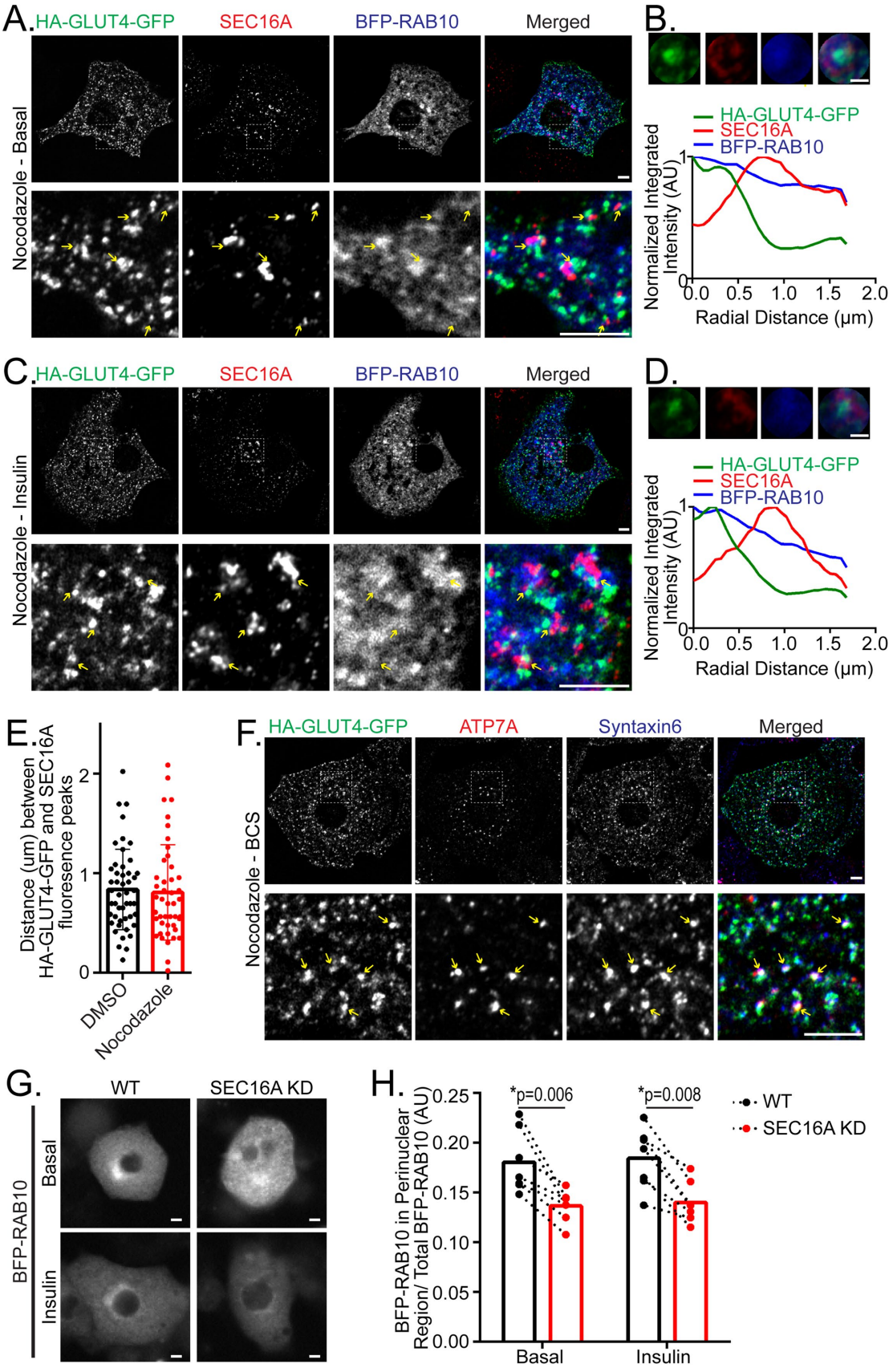

FIGURE 5: The organization of perinuclear RAB10 and SEC16A with GLUT4 has implications for their function in GLUT4 trafficking. (A, C) Representative Airyscan confocal single plane images of cells treated with 3 μM nocodazole. Cells expressing HA-GLUT4-GFP and BFP-RAB10 and stained for endogenous SEC16A by IF. Cells under (A) basal and (C) 1 nM insulin-stimulated conditions. Inset (white, dashed boxed region) is displayed below. Yellow arrows indicate the

polymerization leads to fragmentation and dispersion of the Golgi throughout the cytosol (Cole *et al.*, 1996; Thyberg and Moskalewski, 1999). When the Golgi fragments, Golgi ministacks are formed that retain the structural polarity of the *cis*-, *medial*-, and *trans*-Golgi. The Golgi ministacks are recapitulated at peripheral ERES to re-establish ER to Golgi secretion (Cole *et al.*, 1996). With nocodazole treatment, we observed that the spatial organization of RAB10, SEC16A, and GLUT4 described above was retained under basal and insulin-stimulated conditions (Figure 5, A and C). By performing a radial linescan analysis centered on HA-GLUT4-GFP, we demonstrated SEC16A-labeled membranes remained adjacent to HA-GLUT4-GFP-containing membranes, and RAB10 remained localized with both SEC16A and GLUT4 (Figure 5, B and D). Furthermore, the average distance between peaks of HA-GLUT4-GFP fluorescence and SEC16A fluorescence was approximately 800 nm in both the presence and the absence of nocodazole (Figure 5E). These data suggest that the RAB10-SEC16A-GLUT4 perinuclear organization is not random and could be important for RAB10-SEC16A function in GLUT4 trafficking.

Given that the organization of perinuclear RAB10-SEC16A-GLUT4 is retained with nocodazole treatment, we reasoned that the colocalization of copper transporter ATP7A with GLUT4 at the TGN (Figure 2, A and B) should be retained in fragments formed with nocodazole treatment. Indeed, we observed with nocodazole treatment that ATP7A colocalized with GLUT4 in a subset of GLUT4-containing fragments that contain STX6 (Figure 5F).

Perinuclear SEC16A is important for proper localization of RAB10 at the perinuclear region

Given that SEC16A is known to act as a scaffold for the organization of COPII components at ERES (Whittle and Schwartz, 2010; Sprangers and Rabouille, 2015), we wondered whether perinuclear SEC16A analogously acts as a scaffold for the organization of RAB10 at perinuclear membranes. We found 18% of total BFP-RAB10 localized to the perinuclear region under basal and insulin-stimulated conditions (Figure 5, G and H). Depletion of SEC16A resulted in a 30% decrease in BFP-RAB10 in the perinuclear region under basal and insulin-stimulated conditions (Figure 5, G and H), demonstrating that the presence of the perinuclear pool of SEC16A is important for localizing RAB10 at perinuclear membranes. These data argue that SEC16A-dependent localization of RAB10 at the perinuclear membranes is independent of its GTP/GDP status, and if properly localized at the perinuclear region, RAB10 bound to GTP can carry out its function in insulin-stimulated GLUT4 trafficking.

The RAB10-TBC1D4 module regulates GLUT4 mobilization from the perinuclear region

We next determined if RAB10 and its GAP TBC1D4 regulate the rate of GLUT4 mobilization from the perinuclear region. In cells stably expressing a control shRNA construct, insulin was able to promote mobilization of red HA-GLUT4-mEos3.2 from the perinuclear region (Figure 6A), similar to WT cells (Figure 3E). Depletion of TBC1D4 results in constitutive activation of RAB10 (Sano *et al.*, 2007), and stable knockdown of TBC1D4 in the absence of insulin stimulation led to acceleration of the mobilization of red HA-GLUT4-mEos3.2 from the perinuclear region (Figure 6B) near to the insulin-stimulated rate (Figures 3E and 6A). The effect of TBC1D4 depletion on mobilization of HA-GLUT4-mEos3.2 was rescued by expression of shRNA-resistant TBC1D4 (Figure 6B). Importantly, the accelerated mobilization observed in TBC1D4 knockdown cells was not rescued by expression of a control DNA construct, transferrin receptor (TR) (Figure 6B). In a stable RAB10 knockdown background, insulin stimulation was unable to accelerate the mobilization of HA-GLUT4-mEos3.2 from the perinuclear region, and this phenotype was rescued by expression of BFP-RAB10 in the presence of insulin (Figure 6C). Knockdown of RAB10 under basal conditions had no effect (Figure 6C). Together, these data demonstrate that TBC1D4 regulates mobilization of GLUT4 from the perinuclear region, and RAB10 is required for insulin-stimulated mobilization of GLUT4 from the perinuclear region.

A recent report in HeLa cells demonstrated RAB10 binding to the microtubule motor protein Kinesin 13A/B (KIF13A/B) is required for the tubulation of endosomes (Etoh and Fukuda, 2019). However, in adipocytes, depletion of KIF13A and KIF13B using two different siRNAs alone and in combination did not affect the amount of GLUT4 in the PM under basal or insulin-stimulated conditions compared with WT conditions (Figure 6, D and E). To explore the possibility that RAB10-mediated mobilization of TGN GLUT4 in adipocytes requires a kinesin other than KIF13, we determined whether the effects of RAB10 depletion were additive to those of nocodazole-induced microtubule depolymerization on GLUT4 translocation. Nocodazole treatment resulted in a 50% decrease in the amount of GLUT4 in the PM under insulin stimulation, consistent with previous reports (Olson *et al.*, 2001; Karylowski *et al.*, 2004; Foley and Klip, 2014), and the nocodazole-induced decrease in the amount of GLUT4 in the PM was additive to the effect of RAB10 depletion (Figure 6F). Thus, Rab10-mediated mobilization of GLUT4 from the perinuclear region does not appear to be microtubule-dependent.

DISCUSSION

The data we present supports the hypothesis that the GLUT4 perinuclear storage site is an element of the TGN from which newly synthesized lysosomal proteins are targeted to the late endosomes and the ATP7A copper transporter is translocated to the PM by elevated copper (Figure 7). Consequently, GLUT4 intracellular sequestration and mobilization by insulin is achieved, in part, through utilizing a region of the TGN devoted to specialized transport cargo

same position in each image. Bars, 5 µm. (B, D). Images of the average HA-GLUT4-GFP, SEC16A, and BFP-RAB10 fluorescence intensity from five individual fragments, centered of HA-GLUT4-GFP, resulting from nocodazole treatment from the cells in A and C, respectively. Radial linescan plot of images are displayed below. Values were normalized to each individual fluorescence maxima. Bars, 1 µm. (E) Quantification of the distance (µm) between HA-GLUT4-GFP and SEC16A fluorescence peaks in basal cells in the presence and absence of nocodazole treatment. Values are distances between peaks ± SEM. Distance measured for three separate sets of peaks per cell. $N = 2$ assays, 7–8 cells per assay. (F) Representative Airyscan confocal single plane images of cells treated with 3 µM nocodazole in the presence of 200 µM BCS. Cells expressing HA-GLUT4-GFP and stained for endogenous ATP7A and STX6 by IF. Inset (white, dashed boxed region) is displayed below. Yellow arrows indicate the same position in each image. Bars, 5 µm. (G) Representative images of basal and insulin-stimulated cells expressing BFP-RAB10, siRNA targeting SEC16A electroporated where indicated. Bars, 5 µm. **(H)** Quantification of the fraction of BFP-RAB10 in the perinuclear region of basal and 1 nM insulin-stimulated cells ± addition of siRNA targeting SEC16A. $N = 7$ assays ± SEM. Dashed line connects data from individual assays. *$p < 0.05$, two-tailed unpaired *t* test, nonnormalized raw data. AU, arbitrary units.

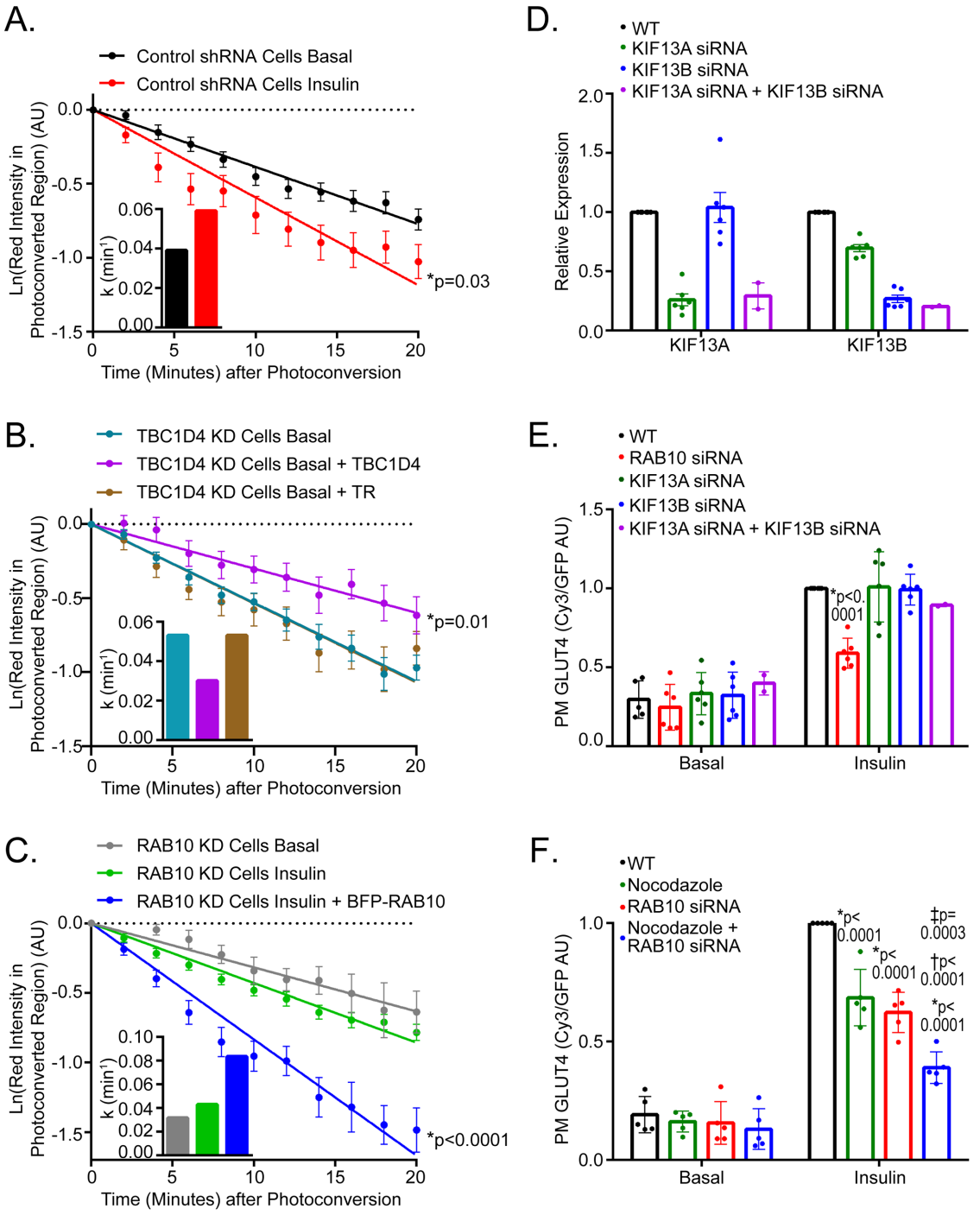

FIGURE 6: The TBC1D4-RAB10 module regulates insulin-stimulated mobilization of GLUT4 from the perinuclear region. (A) Quantification of average red HA-GLUT4-mEos3.2 intensity in the photoconverted perinuclear region of basal and 10 nm insulin-stimulated live cells stably expressing a control shRNA. Values were normalized to value at time 0. Mean normalized values ± SEM, $N = 2$ assays, 6–7 cells per assay. *$p = 0.03$ comparing basal and insulin-stimulated slopes. Inset depicts rate of transport, determined from slope. (B) Quantification of average red HA-GLUT4-mEos3.2 intensity in the photoconverted perinuclear region of basal live cells with stable knockdown of TBC1D4. Cells expressing exogenous TBC1D4 or TR where indicated. Values were normalized to value at time 0. Mean normalized values ± SEM, $N = 3$–7 assays, 5–7 cells per assay. *$p = 0.01$ comparing basal TBC1D4 KD and basal TBC1D4 KD + TBC1D4 slopes. Inset depicts rate of transport, determined from slope. (C) Quantification of average red HA-GLUT4-mEos3.2 intensity in the photoconverted perinuclear region of live cells with stable knockdown of RAB10 under basal and 10 nM insulin-stimulated conditions. Cells expressing exogenous BFP-RAB10 were indicated. Values were normalized to value at time 0. Mean normalized values ± SEM, $N = 2$–6 assays, 4–7 cells per assay. *$p < 0.0001$ comparing insulin-stimulated RAB10 KD and insulin-stimulated RAB10 KD + BFP-RAB10 slopes. Inset depicts rate of transport, determined from slope. (D) Quantitative RT-PCR of relative KIF13A or KIF13B mRNA expression in control 3T3-L1 adipocytes and those electroporated with KIF13A and/or KIF13B siRNAs. $N = 6$ assays. (E) Quantification of PM to total HA-GLUT4-GFP in

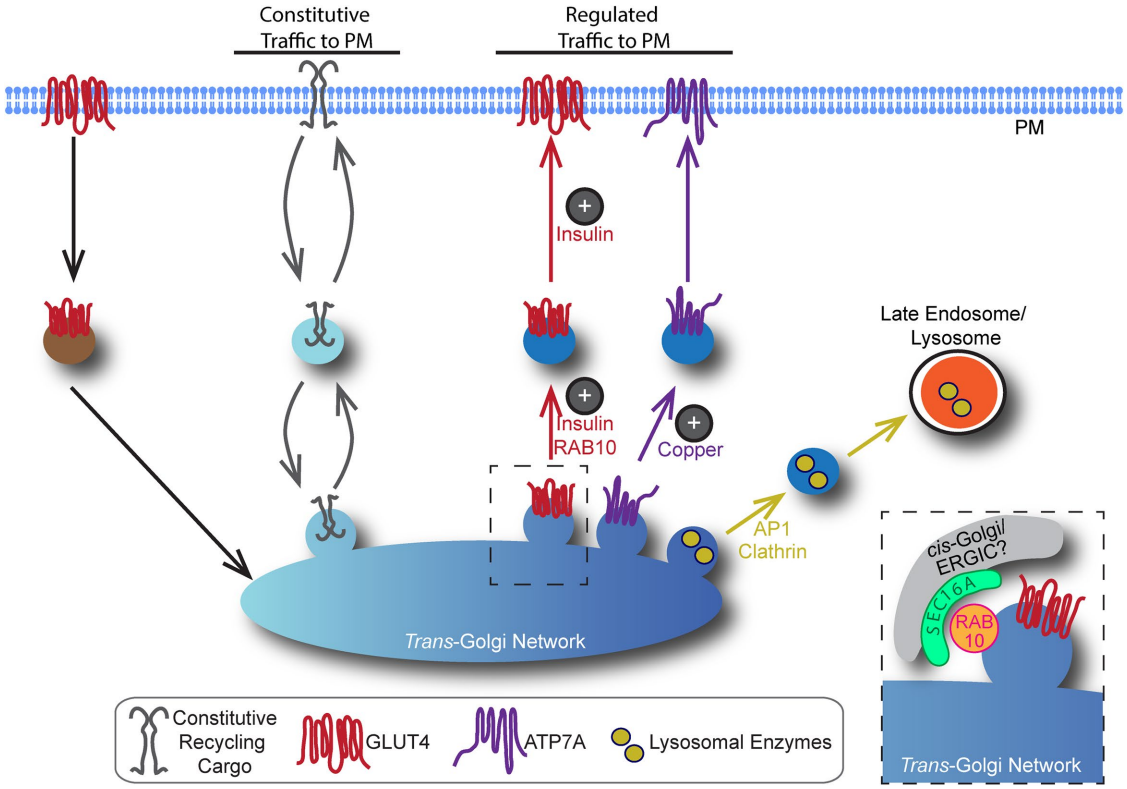

FIGURE 7: Model of GLUT4 trafficking in 3T3-L1 adipocytes. In 3T3-L1 adipocytes, the biogenesis of GLUT4-containing vesicles (IRVs), copper transporter ATP7A-containing vesicles, and vesicles containing lysosomal enzymes occurs at a regulated domain of the TGN; traffic of constitutive recycling proteins through the TGN occurs at an independent domain. Mobilization of ATP7A from the TGN is promoted by copper stimulation. The diversion of vesicles containing lysosomal enzymes away from traffic from the PM is mediated by the AP1 clathrin adaptor. The exocytosis of GLUT4 to the PM is accelerated by insulin. Insulin accelerates the recruitment, docking, and fusion of GLUT4-containing IRVs with the PM. Insulin also promotes the mobilization of GLUT4 from the perinuclear TGN, replenishing the IRV pool. This is important because GLUT4 in the PM is rapidly trafficked back to the TGN via the endosomal pathway. Mobilization of GLUT4 from the perinuclear region is regulated by TBC1D4, and insulin-stimulated acceleration of GLUT4 mobilization requires RAB10. Inset, SEC16A-labeled structures reside adjacent to GLUT4-containing membranes, and SEC16A organizes RAB10 at the perinuclear region.

in general rather than being specific for GLUT4. Our results define this TGN region as a sorting and storage site from which different cargo are mobilized by distinct signals.

Insulin-stimulated acceleration of GLUT4 mobilization from the perinuclear region is regulated by the TBC1D4-RAB10 module

In this study we developed a novel photoconversion and live-cell imaging assay to determine the rates of GLUT4 trafficking to and from the perinuclear compartment under different conditions. We demonstrate in intact cells that insulin accelerates the mobilization of GLUT4 from the perinuclear region by 50%. To date, cell-free in vitro reconstitution assays using extracts of 3T3-L1 adipocytes and muscle cells have provided the best experimental evidence for insulin promoting the formation of IRVs from the TGN (Kristiansen and Richter, 2002; Xu and Kandror, 2002). Incubation of donor membranes (i.e., the TGN) with insulin-stimulated cytosol results in an approximately 50% increase in the biogenesis of IRVs compared with incubation with basal cytosol, consistent with our results in live cells. We find insulin does not regulate GLUT4 recruitment to the perinuclear region. A large portion of GLUT4 in the PM is internalized by clathrin-mediated endocytosis together with constitutively recycling cargo such as TR (Klip *et al.*, 2019). GLUT4-containing endosomes are sent to the TGN, and the observation that delivery of GLUT4 to the TGN is not regulated by insulin is not completely surprising given that insulin stimulation has little effect on TR trafficking (Klip *et al.*, 2019). However, it should be noted that our group has shown that stimulation with insulin results in a small reduction in the rate of GLUT4 internalization at the PM (Blot and McGraw, 2006). This would suggest that endocytosis of GLUT4 at the PM and

serum-starved cells were stimulated with 1 nm insulin. Values were normalized to WT, insulin condition. $N = 2$–6 assays ± SEM. *$p < 0.0001$ compared with WT insulin-stimulated condition (two-way ANOVA followed by Tukey's posttest).
(F) Quantification of PM to total HA-GLUT4-GFP in serum-starved cells were stimulated with 1 nM insulin. siRNA targeting RAB10 electroporated where indicated, and 3 μM nocodazole (or an equivalent volume of DMSO) were added where indicated. Values were normalized to WT, insulin condition. $N = 5$ assays ± SEM. *$p < 0.0001$ compared with WT, insulin condition; †$p < 0.0001$ compared with nocodazole, insulin condition; and ‡$p = 0.0003$ compared with RAB10 KD, insulin condition (two-way ANOVA followed by Tukey's posttest). AU, arbitrary units.

docking/fusion of endocytosed GLUT4-containing vesicles at the TGN are distinct trafficking steps that are differentially regulated. In L6 muscle cells, there is some evidence that insulin stimulation slows GLUT4 internalization (Fazakerley *et al.*, 2010), yet insulin does not affect the rate of arrival of internalized GLUT4 at the STX6-positive TGN in pulse-chase labeling experiments (Foley and Klip, 2014). These data support the idea that there are distinct steps in the trafficking of GLUT4 from the PM to the TGN, much like there are multiple distinct steps in trafficking of GLUT4 from the TGN to the PM.

We demonstrate that the GTPase activating protein TBC1D4 and its target RAB, RAB10, are required for insulin-stimulated mobilization of GLUT4 from the perinuclear region. We find approximately 20% of BFP-RAB10 localizes to the perinuclear region and colocalizes with perinuclear GLUT4, supporting the finding that TBC1D4-RAB10 functions at the perinuclear region. Interestingly, RAB8A, the TBC1D4-target RAB required for insulin-stimulated GLUT4 translocation in muscle, localizes to the perinuclear region in L6 muscle cells (Sun *et al.*, 2014). We cannot exclude that RAB10 functions at the PM in addition to functioning at the TGN as suggested previously (Chen *et al.*, 2012; Sadacca *et al.*, 2013). However, RAB10 functioning at the TGN in GLUT4 trafficking is in line with the function of RAB10 in other systems: RAB10 is involved in TLR4 trafficking from the TGN to the PM (Wang *et al.*, 2010), membrane trafficking from the TGN required for axon development (Liu *et al.*, 2013), and membrane transport to the primary cilia (Babbey *et al.*, 2010).

On insulin stimulation in 3T3-L1 adipocytes, preformed GLUT4 vesicles rapidly dock and fuse with the PM, increasing GLUT4 in the PM until a maximum is reached at 10 min of stimulation (Zeigerer *et al.*, 2002). GLUT4 in the PM is continually internalized and trafficked to the TGN. Accelerating the formation of IRVs that can be trafficked to the PM allows the increase in PM GLUT4 to be maintained at longer lengths of insulin stimulation (Zeigerer *et al.*, 2002). Expression of a dominant-negative TBC1D4 construct (TBC1D4-DN), which is mutated in four of the six AKT phosphorylation sites, blocks the RAB10-regulated GLUT4 trafficking step (Sano *et al.*, 2003). In cells expressing TBC1D4-DN, insulin transiently increases GLUT4 in the PM within 5 min of stimulation; however, this increase cannot be maintained at longer lengths of insulin stimulation (Eguez *et al.*, 2005). Furthermore, with TBC1D4-DN expression, insulin-stimulated recruitment of GLUT4 to the PM is biphasic, with rapid exocytosis of 40% of GLUT4, followed by slow exocytosis of the remaining GLUT4 (Eguez *et al.*, 2005). The ability of insulin to initially recruit GLUT4 to the PM indicates that insulin promotes the recruitment, docking, and fusion of preformed GLUT4 vesicles, and thus the regulation of these steps is not directly dependent on TBC1D4-RAB10. Furthermore, at basal state, approximately half of GLUT4 resides in vesicles (Roccisana *et al.*, 2013), consistent with the observed rapid exocytosis of 40% of GLUT4 on insulin stimulation. The inability of insulin to maintain the initial increase in GLUT4 in the PM, and the inefficient exocytosis of 60% of GLUT4, suggests that insulin no longer has a pool of IRVs to pull on because the pool of preformed GLUT4 vesicles has been depleted and the IRV pool has not been efficiently repopulated through accelerated mobilization of GLUT4 from the TGN. The inability of insulin to promote the mobilization of GLUT4 from the TGN in nascent IRVs in cells expressing TBC1D4-DN is consistent with TBC1D4-RAB10 regulating this step. Interestingly, in 3T3-L1 fibroblasts insulin stimulation transiently increases the amount of GLUT4 in the PM within 10 min of stimulation; however, this increase cannot be maintained over longer lengths of stimulation (Govers *et al.*, 2004). One explanation of these data is that 3T3-L1 fibroblasts express the machinery required for insulin-stimulated increase in efficiency of IRV docking and fusion with the PM; however, they do not express the machinery required for insulin-stimulated mobilization of GLUT4 from the perinuclear compartment. The expression of such machinery may be gained throughout differentiation.

Although we have established mobilization of GLUT4 from the TGN as an insulin-controlled step dependent on TBC1D4/RAB10, we have not as yet defined the mechanism of GLUT4 mobilization. Insulin signaling could accelerate the biogenesis of IRVs at the TGN, or insulin signaling could accelerate the movement of newly formed IRVs from the perinuclear area. The latter could be accomplished by linking nascent IRVs to the cytoskeleton at the perinuclear region. The kinesin motors KIF5B (Semiz *et al.*, 2003) and KIF3 (Imamura *et al.*, 2003) have been suggested to be required for insulin-stimulated GLUT4 translocation, and RAB10 interaction with KIF13A and KIF13B has recently been shown to be required for tubulation of endosomes in HeLa cells (Etoh and Fukuda, 2019). However, we find that effects of nocodazole-induced microtubule depolymerization and siRNA-mediated depletion of RAB10 on insulin-stimulated GLUT4 translocation are additive, arguing that RAB10-mediated mobilization of GLUT4 from the perinuclear region is not dependent on microtubules. RAB10 has been shown to interact with the myosin motor MYO5A (Roland *et al.*, 2011), and RAB10-MYO5A interaction has been suggested to regulate IRV docking/fusion in adipocytes (Chen *et al.*, 2012). Interestingly, in muscle MYO5A interaction with RAB8A is argued to regulate GLUT4 trafficking at the perinuclear region (Sun *et al.*, 2014). Furthermore, in neurons, RAB10 interaction with MYO5B is required for the fission of RAB10 vesicles at the TGN (Liu *et al.*, 2013). Thus, it may be useful to think about RAB10 possibly interacting with myosin motors to regulate IRV formation and/or link them to the cytoskeletal system. Of note, KIF13B, KIF5B, and MYO5A were present in immunoabsorbed GLUT4-containing membranes; however, none were differentially immunoabsorbed in F^5Y-GLUT4 membranes.

SEC16A is important for RAB10 localization at the perinuclear region

Here we have advanced the understanding of the role of SEC16A in GLUT4 trafficking. We show the previously described SEC16A-labeled structures that surround GLUT4 in the perinuclear TGN (Bruno *et al.*, 2016) are also associated with RAB10. The spatial organization of perinuclear GLUT4-SEC16A-RAB10 is not random. Nocodazole depolymerization of microtubules disperses GLUT4 (Cole *et al.*, 1996; Thyberg and Moskalewski, 1999), yet the organization of GLUT4-SEC16A-RAB10 is retained. The distance between adjacent peaks of GLUT4 and SEC16A is approximately 800 nm with or without nocodazole treatment, and RAB10 remains colocalized with GLUT4 and SEC16A. A peak-to-peak distance of 800 nm is in line with the average diameter of a Golgi cisternae, which has been calculated to range from 500 to 1000 nm (Klumperman, 2011). We further find that siRNA-mediated depletion of SEC16A results in a 30% reduction of RAB10 in the perinuclear region under basal and insulin-stimulated states. These data argue SEC16A is important for localizing RAB10 to the perinuclear region, and SEC16A can bind to RAB10 whether it is bound to GDP or GTP. These data are consistent with the known role of SEC16A at ERES, where it acts as a scaffold for organization of COPII components (Whittle and Schwartz, 2010; Sprangers and Rabouille, 2015).

Mutations in the leucine-rich repeat kinase 2 (LRRK2) are associated with Parkinson's disease (PD). LRRK2 has been suggested to regulate SEC16A localization at ERES (Cho *et al.*, 2014). More recently, LRRK2 has been shown to phosphorylate a subset of RAB

proteins, including RAB10 (Steger *et al.*, 2016). RAB10 phosphorylation status at LRRK2 sites has been implicated in regulation of ciliogenesis and expression of mutant LRRK2 with defects in ciliogenesis (Dhekne *et al.*, 2018; Lara Ordonez *et al.*, 2019). It will be interesting to determine if PD-associated mutations in LRRK2 have any effect on GLUT4 trafficking in adipocytes.

A role for the GLUT4-containing TGN in the biogenesis and sorting of specialized vesicular carriers

We identified the protein composition of the GLUT4-containing TGN by identifying proteins enriched in F^5Y-GLUT4 immunoabsorption compared with WT and F^5A-GLUT4-containing immunoabsorption. The enrichment of lysosomal enzymes known to traffic from the TGN to late endosomes/lysosomes and the ATP7A copper transporter without an enrichment for proteins targeted to the PM, the default pathway from the TGN, led us to conclude that IRVs form from a region of the TGN where transport vesicles containing specialized cargos form. Various studies support the notion that the TGN is comprised of molecularly distinct subdomains (Derby *et al.*, 2004; Brown *et al.*, 2011; Tie *et al.*, 2018). We do not know if the detergent-free cell lysis method used in the immunoabsorption of GLUT4-containing compartments isolates individual stacks or fragments of stacks. However, the enriched immunoabsorption of cargo whose trafficking is specialized, but not constitutively recycling cargo, argues that the method distinguishes different regions or subdomains of the TGN.

Interestingly, when GLUT4 is ectopically expressed in cell types that do not natively express GLUT4, such as fibroblasts, CHO cells, and HeLa cells, an insulin-regulated recycling mechanism does exist, albeit less robust than in adipocytes (Lampson *et al.*, 2001; Camus *et al.*, 2020). Specifically, it has been demonstrated that GLUT4 travels to the PM in vesicles that are distinct from vesicles carrying constitutively recycling cargo (Lampson *et al.*, 2001). The ATP7A copper transporter is more widely expressed than is GLUT4. Hence, the specialized TGN subdomain that contains GLUT4 and ATP7A in 3T3-L1 adipocytes likely exists in other cell types that do not natively express GLUT4, explaining why there is rudimentary insulin-regulation of GLUT4 traffic when it is ectopically expressed in these other cell types.

Two major destinations for proteins in the TGN are the late endosome/lysosome and the PM. The MPR and AP1 clathrin adaptin complex are required for diverting cargo destined for the late endosome/lysosome away from the PM (Braulke and Bonifacino, 2009). Their enrichment in F^5Y-GLUT4-containing perinuclear compartments argues that the GLUT4-containing TGN is the site where lysosomal enzymes are sorted into specialized transport vesicles that traffic to the late endosome/lysosome. Previous immunofluorescence (IF) and electron microscopy studies have demonstrated that GLUT4 colocalizes with MPR (Martin *et al.*, 2000a) and AP1 (Martin *et al.*, 2000b), validating their enrichment. Trafficking of the copper transporter ATP7A between the TGN and the PM is known to be tightly regulated by copper load to maintain copper homeostasis (Petris *et al.*, 1996). Enrichment of ATP7A in F^5Y-GLUT4-containing perinuclear compartments argues that the GLUT4-containing TGN is also the site where select regulated recycling membrane proteins are packaged in transport vesicles that travel to the PM. Colocalization of ATP7A with GLUT4 in the TGN is supported by the observation that with nocodazole treatment, ATP7A remains colocalized with GLUT4 in a subset of fragments. Airyscan confocal microscopy studies that have looked at the localization of various TGN markers in nocodazole-induced ministacks did not show significant colocalization of many of the markers (Tie *et al.*, 2018). The authors argue that their data are consistent with there being subdomains of the TGN that possess unique molecular identities. Based on this logic, observing colocalization of ATP7A, GLUT4, and STX6 in nocodazole-induced fragments would suggest they occupy a distinct TGN subdomain. It is provocative to think a particular protein may be important for maintaining the architecture of a TGN subdomain and consequently be important for keeping ATP7A and GLUT4 together in nocodazole-induced ministacks. For example, the TGN golgin proteins have been shown to localize to different subdomains of the TGN containing specific cargo (Brown *et al.*, 2011; Derby *et al.*, 2004) and suggested to be important for maintaining the structure of the particular subdomain they localize to (Derby *et al.*, 2004). ATP7A is mobilized from the GLUT4-containing TGN in response to elevated copper, but not insulin stimulation. On the other hand, copper stimulation does not induce translocation of GLUT4. Furthermore, dual stimulation with copper and insulin does not result in additive effects on mobilization of ATP7A or GLUT4 translocation. These data demonstrate that stimuli mobilize specific cargo from the GLUT4-containing TGN. Depletion of RAB10 does not blunt copper-elicited mobilization of ATP7A from the perinuclear region, demonstrating that different stimuli mobilize specific cargo through distinct molecular machinery.

Proteins localized to the TGN and TGN transport vesicles were the most significantly enriched in F^5Y-GLUT4-containing perinuclear compartments. However, there was also an enrichment of endosome, Golgi, and ERGIC proteins. These compartments are found in the compact perinuclear region, raising the possibility that the packaging and sorting of cargo in transport vesicles at the perinuclear region involves the interplay of membrane compartments of different natures. In human cells, a clathrin heavy chain isoform, CHC22, has been proposed to function at the ERGIC to sequester newly synthesized GLUT4 in IRVs (Camus *et al.*, 2020). Mice do not have an equivalent CHC22 gene and it has been suggested that CHC17 isoform might substitute for CHC22 in regulation of GLUT4 in mice (Camus *et al.*, 2020). It is of interest to note that mouse CHC protein (CLTC)/ CHC17 was one of the most abundant proteins based on signal intensity in all four immunoabsorption experiments, although CLTC was not differentially absorbed in any of the comparisons. Clathrin is required for AP1-mediated vesicle trafficking between the TGN and the late endosome, and therefore immunoisolation of clathrin with GLUT4 is consistent with GLUT4 localization to the region of the TGN where AP1-containing vesicles are formed.

Taken together, the data presented serve to refocus the understanding of insulin control of GLUT4 in adipocytes to include events deep in the cell at the TGN, not just PM proximal events. Demonstrating insulin promotes the mobilization of GLUT4 from a molecularly unique TGN storage site through RAB10 activity provides important insight into the trafficking of GLUT4 and other cargoes at the TGN, and also provides incentive to investigate the mechanisms at work in more detail.

MATERIALS AND METHODS

Request a protocol through Bio-protocol.

cDNA constructs, siRNA, antibodies, chemicals, and drugs

cDNA constructs encoding WT, F^5Y, F^5A-HA-GLUT4-GFP, TR, and TBC1D4 have been previously described (Lampson *et al.*, 2000; Sano *et al.*, 2003; Blot and McGraw, 2006). The HA-GLUT4-mEos3.2 cDNA construct was generated by replacing GFP in the HA-GLUT4-GFP cDNA construct for mEos3.2 (Addgene plasmid #54525) (Zhang *et al.*, 2012) through restriction cloning. *Kpn*I and *Bam*HI restriction sites respectively flank the N- and C-terminuses of GFP. A

wobble mutation was made at an internal *Kpn*I site in mEos3.2 to prevent its digestion using the QuikChange II XL Site-Directed Mutagenesis kit (200521; Agilent Technologies) and following primer pair: 5′-GTT CGA TTT TAT GGT ACT AAC TTT CCC GCC AAT GG-3′ and 5′-CCA TTG GCG GGA AAG TTA GTA CCA TAA AAT CGA AC-3′. mEos3.2 with the wobble internal *Kpn*I site was PCR amplified with an N-terminal primer containing a *Kpn*I restriction site: 5′-GCTTGGTACCATGAGTGCG-3′, and C-terminal primer containing a *Bam*HI restriction site: 5′-GCTAGGATCCTTATCGTCTGGC-3′. The BFP-RAB10 cDNA construct was a kind gift from Gia Voeltz at University of Colorado Boulder.

Antibodies against STX6 (ab12370; Abcam and 2869T; Cell Signaling), TGN46 (ab16059; Abcam), LAMP1 (ab25630; Abcam), ATP7A (LS-C209614; LSBio), GM130 (610822; BD Transduction), SEC16A (KIAA0310; ProteinExpress), and hemagglutinin (HA) tag (901503; BioLegend) were used for IF. Antibodies against GFP (11814460001; Sigma-Aldrich), ATP7A (LS-C209614; LSBio), RAB10 (4262S; Cell Signaling), STX6 (ab12370; Abcam), TGN46 (ab16059; Abcam), and Actin (AAN01-A; Cytoskeleton) were used for Western blotting.

Chemicals and drugs used were MK-2206 (11593; Cayman), nocodazole (M1404; Sigma-Aldrich), BCS (B1125-500MG; Sigma-Aldrich), and Copper(II) chloride dehydrate (C3279; Sigma-Aldrich).

The siRNA constructs targeting RAB10 and SEC16A were as previously published. RAB10: si251, 5′-GCA UCA UGC UAG UGU AUGA-3′ (same sequence as shRNA expressed by RAB10 KD cells; Sano *et al.*, 2007). SEC16A: si1, 5′-CTT CAG AAT ATC AGC TCC CTG GGG CTC-3′, si3, 5′-AGC TGG ACT TGC TGG TGG CTG GGC CAA-3′ (Bruno *et al.*, 2016) (two siRNA were used to target SEC16A to achieve a greater reduction in RNA). The siRNAs for KIF13A and KIF13B were designed at Integrated DNA Technologies. KIF13A: si2, 5′-ATC CTT TAA ATA GTA AAC CAG AAG CTC-3′. KIF13B: si2, 5′-CAC ATT TGG TAT GTA AGT CAA TTT CTC-3′.

Cell lines and culture

The 3T3-L1 preadipocytes (fibroblasts) were cultured and differentiated into adipocytes as previously described (Zeigerer *et al.*, 2002). The cells were originally received from G. Baldini (University of Arkansas) in 1992. These cells were last tested for mycoplasma in 2017. Experiments were performed on day 5 after differentiation. The 3T3-L1 adipocyte cell lines stably expressing shRNA sequences against RAB10 or TBC1D4 and expressing control shRNA sequences that do not target genes in the mouse genome have been described previously (Eguez *et al.*, 2005; Sano *et al.*, 2007).

Immunoabsorption experiments were performed using 3T3-L1 cell lines stably expressing WT and mutant HA-GLUT4-GFP. To generate these cell lines, cDNA constructs encoding WT, F^5Y, and F^5A-HA-GLUT4-GFP (Lampson *et al.*, 2000; Blot and McGraw, 2006) were subcloned into the pLenti6/V5-D-TOPO vector (K4955-10; Life Technologies). The 293FT packaging cells were transfected with lentiviral cDNA using Lenti-X packaging system (631276; Takara). Cultured media containing lentiviral particles were harvested after 72 h and used to infect 3T3-L1 preadipocytes. HA-GLUT4-GFP-positive cells were sorted by FACS and cultured in selection medium supplemented with blasticidin (A11139-03; Invitrogen).

Electroporation of adipocytes

Differentiated 3T3-L1 adipocytes were electroporated with 45–55 µg of cDNA constructs as described previously (Zeigerer *et al.*, 2002). Adipocytes were electroporated with 2 nmol of siRNA where indicated. When two siRNAs were used, 2 nmol of each siRNA was electroporated. Assays were performed 12–72 h postelectroporation as described.

Quantitative RT-PCR

Measurement of KIF13A and KIF13B siRNA-mediated knockdown was performed by quantitative RT-PCR. At 72 hours postelectroporation, cells were harvested, RNA was extracted using the RNeasy kit (74106; QIAGEN), and cDNA was prepared from extracted RNA using the RNA to cDNA EcoDry Premix (639545; Takara Bio). Quantitative RT-PCR was performed using appropriate primer pairs from the PrimerBank database. Primer pair to KIF13A: forward, 5′-TCG GAT ACG AAG GTA AAA GTT GC-3′ and reverse, 5′-CTG CTT AGT GTT GGA AGG AGG-3′. Primer pair to KIF13B: forward, 5′-GCT CTG TAG TGG ACT CTT TGA AC-3′ and reverse, 5′-TTT GGG GTC AAG AAG GTC TCG-3′.

GLUT4 translocation (surface to total)

HA-GLUT4-GFP has a HA-epitope engineered into the first exofacial loop and GFP fused to its cytoplasmic carboxyl domain. The amount of the reporter in the PM of individual cells was determined by anti-HA IF, normalized to the GFP fluorescence. GLUT4 translocation assay was performed as described previously (Lampson *et al.*, 2000). Briefly, cells expressing HA-GLUT4-GFP were incubated in serum-free media for 2 h. Cells were stimulated with 1 or 10 nM insulin for 30 min to achieve steady state GLUT4 surface levels. Cells were fixed with 3.7% formaldehyde for 6–10 min, and an anti-HA antibody (901503; BioLegend) was used, without permeabilization, to label HA-GLUT4-GFP on the cell surface. HA staining was visualized with Cy3 fluorescently tagged secondary antibody (115-165-062; Jackson Immunoresearch), and total HA-GLUT4-GFP was visualized by direct fluorescence, as described later.

Copper transporter ATP7A mobilization assay

HA-GLUT4-GFP expressing cells were treated with 200 µM BCS for 2 h to achieve low copper conditions, followed by stimulation with 200 µM Copper(II) chloride dehydrate for 2 h or 1 nM insulin for 30 min. For dual stimulation, following BCS treatment, cells were stimulated with Copper(II) chloride dehydrate for 1.5 h, followed by treatment with Copper(II) chloride dehydrate and insulin for 30 min. Cells were fixed and stained for native ATP7A and STX6 in the presence of 0.5 mg/ml saponin.

HA-GLUT4-mEos3.2 photoconversion assay

HA-GLUT4-mEos3.2-expressing cells were serum starved for 2 h in live-cell imaging media containing DMEM without phenol red (D5030; Sigma-Aldrich) and supplemented with 4500 mg/l D-glucose (G7528; Sigma-Aldrich), 4 mM L-glutamine (G8540; Sigma-Aldrich), 4.76 g/l HEPES (H3375; Sigma-Aldrich), 1 mM sodium pyruvate (11360, Life Technologies), and 2.5g/l sodium bicarbonate (S6297; Sigma-Aldrich) at pH 7.2. Where indicated, cells were subsequently stimulated with 10 nM insulin for 10 min. Cells were then transferred to the confocal microscope where they were housed in an incubation chamber at 37°C, 5% CO_2. Setup on the scope took approximately 5 min once the sample was placed, thus making the total incubation time in insulin prior to photoconversion 15 min (at 15 min of insulin stimulation, cells have achieved insulin-stimulated steady state conditions). For experiments where the AKT inhibitor MK2206 was added, cells were treated with 1 µM MK2206, or equivalent volume of DMSO, for the last hour of the starvation period, as well as during the 15-min incubation period with insulin (75 min total).

Microscopy, image quantification, and statistical analysis

Epifluorescence. Epifluorescence images were collected on an inverted microscope at room temperature using a 20× air objective (Leica Biosystems) and a cooled charge-coupled device 12-bit

camera. Exposure times and image quantification (Lampson *et al.*, 2001) were performed using MetaMorph image processing software (Universal Imaging) as previously described. GFP and Cy3 fluorescence signals were background corrected and the surface(Cy3)/total(GFP) (S/T) GLUT4 was calculated for each cell. The S/T values were normalized within each assay to the mean S/T value for the indicated condition to allow for averaging results across multiple biological repeat assays. For statistical analysis, a one-way or two-way ANOVA followed by Tukey's multiple comparison tests were carried out in Prism as indicated in the figure legends. To quantify the fraction of BFP-RAB10 in the perinuclear region, cells were cotransfected with HA-GLUT4-GFP. Perinuclear HA-GLUT4-GFP was used as a marker to create an outline of the perinuclear region, and the outline was transferred to the image of BFP-RAB10. As a measure of the fraction of BFP-RAB10 in the perinuclear region, the integrated BFP-RAB10 intensity in the outlined perinuclear region was calculated and divided by the total integrated intensity of BFP-RAB10 in the cell. Unpaired Student's *t* tests were performed on raw (nonnormalized) S/T mean values from multiple assays.

Airyscan confocal experiments. Airyscan confocal images were collected on a laser scanning microscope (LSM880; ZEISS) with Airyscan using a 63× objective. For quantification of percent overlap of protein x with protein y, a threshold using the 98th percentile grayscale value was set on the image of protein x and on the image of protein y. A binary mask of the thresholded protein y was generated, and percent of thresholded protein x intensity under the mask was calculated. For statistical analysis, a one-way ANOVA followed by Tukey's multiple comparison tests were carried out in Prism.

Linescan analyses. Linescan plots were generated using the Linescan application in MetaMorph or ImageJ. Radial linescan plots were generated using the Radial Profile Plot plugin in ImageJ (https://imagej.nih.gov/ij/plugins/radial-profile.html). For each radial linescan plot, five HA-GLUT4-GFP fragments were selected based on high HA-GLUT4-GFP intensity. A circle with a radius of 40 pixels was applied to the fragment and centered on the peak of HA-GLUT4-GFP fluorescence. A plot of normalized integrated HA-GLUT4-GFP, SEC16A, and BFP-RAB10 fluorescence intensities around the circle (sum of integrated pixel values around circle/ total number of pixels) (*y*-axis) was plotted for each distance from the center of the circle (*x*-axis).

HA-GLUT4-mEos3.2 photoconversion and live-cell imaging. Photoconversion of HA-GLUT4-mEos3.2 and image collection were performed on a laser scanning microscope (LSM880; ZEISS) with incubation chamber using a 63× objective. Green and red prephotoconversion images of a cell expressing HA-GLUT4-mEos3.2 were acquired by excitation with 488- and 561-nm lasers, respectively. A high scan speed of 10, no averaging, and a low laser power of 0.2% were used to prevent photobleaching. A designated section of the perinuclear region was then bleached with a 405-nm laser at 20% power, scan speed of 7 for 12 cycles. Green and red postphotoconversion images of the cell expressing HA-GLUT4-mEos3.2 were acquired every 2 min for a total of 20 min. The definite focus option was used in an attempt to prevent drift in the *z*-axis. For the average red intensity value in the photoconverted region at each time point postphotoconversion, the prephotoconversion red intensity value was subtracted in MetaMorph. Values were then normalized to the 0 min postphotoconversion value and the natural log was taken. After averaging across multiple cells, a linear curve fit was applied. Statistical comparison of slopes was performed in Prism by calculating a two-tailed *p* value from testing the null hypothesis that the slopes are identical. For the average green intensity value at each time point postphotoconversion, the prephotoconversion green intensity value was subtracted. Values were then normalized to the negative value of the 0 min time point postphotoconversion and added to 1. After averaging across multiple cells, an exponential curve fit was applied.

Immunoisolation of native GLUT4-containing compartments, SILAC mass spectrometry, and data processing. Each pairwise comparison was performed in inverted forward and reverse labeling conditions. For the WTvsF^{5}Y comparison, the labeling design was 1) forward condition: WT HA-GLUT4-GFP cells grown in light SILAC medium versus F^{5}Y-HA-GLUT4-GFP cells grown in heavy SILAC medium, and 2) reverse condition: WT HA-GLUT4-GFP cells grown in heavy SILAC medium versus F^{5}Y-HA-GLUT4-GFP cells grown in light SILAC medium. For the F^{5}YvsF^{5}A comparison, the labeling design was 1) forward condition: F^{5}Y-HA-GLUT4-GFP cells grown in light SILAC medium versus F^{5}A-HA-GLUT4-GFP cells grown in heavy SILAC medium and 2) reverse condition: F^{5}Y-HA-GLUT4-GFP cells grown in heavy SILAC medium versus F^{5}A-HA-GLUT4-GFP cells grown in light SILAC medium.

The objective of this experiment was to identify by SILAC mass spectrometry proteins colocalized with GLUT4 in the perinuclear compartment based on enrichment with F^{5}Y-GLUT4 in immunoabsorption, not to identify all proteins in GLUT4-containing compartments. Therefore, we did not include a control condition to identify proteins that are nonspecifically absorbed during the immunoisolation.

Stable isotope labeling of cultured cells. Stable HA-GLUT4-GFP-expressing 3T3-L1 preadipocytes were grown for five doublings and differentiated in lysine (LYS) and arginine (ARG)-deficient DMEM (89985; Thermo Scientific), supplemented with 10% dialyzed fetal bovine serum and 42 µg/ml either LYS-HCL and ARG-HCL normal isotopes (light SILAC medium) or with $^{13}C_6$LYS and $^{13}C_6$LYS,$^{15}N_4$ ARG isotopes (heavy SILAC medium) (89983 and 88210; Pierce) at 37°C in 5% CO_2. Under these conditions, the isotopes incorporation efficiency was higher than 95%, without detectable ARG to proline conversion.

Immunoisolation of GLUT4-containing compartments. Day 5 postdifferentiation, labeled stable HA-GLUT4-GFP-expressing 3T3-L1 adipocytes were incubated in serum-free either light or heavy SILAC media for 2 h at 37°C in 5% CO_2 to establish basal GLUT4 retention. Cells were washed one time with phosphate-buffered saline (PBS), harvested into 1 ml of HES buffer (20 mM HEPES, 1 mM EDTA, 250 mM sucrose, and protease inhibitors), and homogenized by subsequent passage through 22G$^{1/2}$ and 27G$^{1/2}$ syringes on ice. Total cell homogenates were cleared by successive centrifugations at 1000 × *g* for 10 min to remove unbroken cells, nuclei, and fat. Protein concentration of both light-cultured cells and heavy-cultured cells was measured by BCA assay (23225; Thermo Scientific) and homogenates were mixed to a 1:1 ratio. HA-GLUT4-GFP-containing compartments were isolated by incubation for 30 min at 4°C with magnetic GFP-bound beads (130-091-125; Miltenyi Biotec). Beads were washed 5× in PBS supplemented with protease inhibitors and absorbed material was eluted with elution buffer (50 mM Tris HCl [pH 6.08], 50 mM dithiothreitol, 1% SDS, 1 nM EDTA, 0.005% bromophenol blue, 10% glycerol). For immunoblots, WT HA-GLUT4-GFP-containing compartments were immunoisolated from cells

stably expressing WT HA-GLUT4-GFP according to the procedure above. Standard Western blotting protocols were used.

LC-MS/MS and bioinformatics analysis. Eluates were resolved on a 5–20% gradient SDS–PAGE gel and subjected to in-gel digest followed by LC-MS/MS analysis as described (Graumann *et al.*, 2008). Peptide/spectrum matching as well as false discovery control (1% on the peptide and protein levels, both) and protein quantitation were performed using the MaxQuant suite of algorithms (Cox and Mann, 2008). We used the SILAC ratio of polypeptides in the immunoabsorbates to identify proteins enriched with F^5Y-GLUT4. The comparisons of F^5Y to WT and F^5Y to F^5A were performed twice, switching which sample was labeled with heavy amino acids. We identified the proteins whose average ratios in the two F^5Y versus WT and F^5Y versus F^5A experiments were greater than 1.3-fold with a "significance B" (Cox and Mann, 2008) < 0.05, falling back on the method due to the small *n*. There were 508 proteins enriched in the F^5Y versus the combined WT and F^5A data sets. We used the merged data set for downstream computational analyses.

ACKNOWLEDGMENTS

We thank Leona Cohen-Gould and Sushmita Mukherjee at the Weill Cornell Medicine Optical Microscopy Core where confocal microscopy was performed and Harold Skip Ralph at the Weill Cornell Medicine Automated Optical Microscopy Core for help with image analysis. We thank Gus Lienhard (Dartmouth Medical School), Maria Belen Picatoste Botija, Rosemary Leahey, Anudari Letian, Anuttoma Ray, Lucie Yammine, and Eyoel Yemanaberhan for helpful discussions and critically reading the manuscript. This research was supported by National Institutes of Health (NIH) RO1 DK52852 (T.E.M.), NIH DK125699 (T.E.M.), NIH 5T32 GM008539 (A.B.), and an American Diabetes Association mentor-based fellowship award to T.E.M.

REFERENCES

Ashburner M, Ball CA, Blake JA, Botstein D, Butler H, Cherry JM, Davis AP, Dolinski K, Dwight SS, Eppig JT, *et al.* (2000). Gene ontology: tool for the unification of biology. The Gene Ontology Consortium. Nat Genet 25, 25–29.

Babbey CM, Bacallao RL, Dunn KW (2010). Rab10 associates with primary cilia and the exocyst complex in renal epithelial cells. Am J Physiol Renal Physiol 299, F495–F506.

Bai L, Wang Y, Fan J, Chen Y, Ji W, Qu A, Xu P, James DE, Xu T (2007). Dissecting multiple steps of GLUT4 trafficking and identifying the sites of insulin action. Cell Metab 5, 47–57.

Blot V, McGraw TE (2006). GLUT4 is internalized by a cholesterol-dependent nystatin-sensitive mechanism inhibited by insulin. EMBO J 25, 5648–5658.

Blot V, McGraw TE (2008a). Molecular mechanisms controlling GLUT4 intracellular retention. Mol Biol Cell 19, 3477–3487.

Blot V, McGraw TE (2008b). Use of quantitative immunofluorescence microscopy to study intracellular trafficking: studies of the GLUT4 glucose transporter. Methods Mol Biol 457, 347–366.

Braulke T, Bonifacino JS (2009). Sorting of lysosomal proteins. Biochim Biophys Acta 1793, 605–614.

Brown FC, Schindelhaim CH, Pfeffer SR (2011). GCC185 plays independent roles in Golgi structure maintenance and AP-1-mediated vesicle tethering. J Cell Biol 194, 779–787.

Bruno J, Brumfield A, Chaudhary N, Iaea D, McGraw TE (2016). SEC16A is a RAB10 effector required for insulin-stimulated GLUT4 trafficking in adipocytes. J Cell Biol 214, 61–76.

Camus SM, Camus MD, Figueras-Novoa C, Boncompain G, Sadacca LA, Esk C, Bigot A, Gould GW, Kioumourtzoglou D, Perez F, *et al.* (2020). CHC22 clathrin mediates traffic from early secretory compartments for human GLUT4 pathway biogenesis. J Cell Biol 219, e201812135.

Chen Y, Wang Y, Zhang J, Deng Y, Jiang L, Song E, Wu XS, Hammer JA, Xu T, Lippincott-Schwartz J (2012). Rab10 and myosin-Va mediate insulin-stimulated GLUT4 storage vesicle translocation in adipocytes. J Cell Biol 198, 545–560.

Cho HJ, Yu J, Xie C, Rudrabhatla P, Chen X, Wu J, Parisiadou L, Liu G, Sun L, Ma B, *et al.* (2014). Leucine-rich repeat kinase 2 regulates Sec16A at ER exit sites to allow ER-Golgi export. EMBO J 33, 2314–2331.

Cole NB, Sciaky N, Marotta A, Song J, Lippincott-Schwartz J (1996). Golgi dispersal during microtubule disruption: regeneration of Golgi stacks at peripheral endoplasmic reticulum exit sites. Mol Biol Cell 7, 631–650.

Consortium TGO (2019). The Gene Ontology Resource: 20 years and still GOing strong. Nucleic Acids Res 47, D330–D338.

Cox J, Mann M (2008). MaxQuant enables high peptide identification rates, individualized p.p.b.-range mass accuracies and proteome-wide protein quantification. Nat Biotechnol 26, 1367–1372.

Derby MC, van Vliet C, Brown D, Luke MR, Lu L, Hong W, Stow JL, Gleeson PA (2004). Mammalian GRIP domain proteins differ in their membrane binding properties and are recruited to distinct domains of the TGN. J Cell Sci 117, 5865–5874.

Dhekne HS, Yanatori I, Gomez RC, Tonelli F, Diez F, Schule B, Steger M, Alessi DR, Pfeffer SR (2018). A pathway for Parkinson's Disease LRRK2 kinase to block primary cilia and Sonic hedgehog signaling in the brain. Elife 7.

Eguez L, Lee A, Chavez JA, Miinea CP, Kane S, Lienhard GE, McGraw TE (2005). Full intracellular retention of GLUT4 requires AS160 Rab GTPase activating protein. Cell Metab 2, 263–272.

Etoh K, Fukuda M (2019). Rab10 regulates tubular endosome formation through KIF13A and KIF13B motors. J Cell Sci 132.

Fazakerley DJ, Holman GD, Marley A, James DE, Stockli J, Coster AC (2010). Kinetic evidence for unique regulation of GLUT4 trafficking by insulin and AMP-activated protein kinase activators in L6 myotubes. J Biol Chem 285, 1653–1660.

Foley KP, Klip A (2014). Dynamic GLUT4 sorting through a syntaxin-6 compartment in muscle cells is derailed by insulin resistance-causing ceramide. Biology Open 3, 314–325.

Foster LJ, Li D, Randhawa VK, Klip A (2001). Insulin accelerates inter-endosomal GLUT4 traffic via phosphatidylinositol 3-kinase and protein kinase B. J Biol Chem 276, 44212–44221.

Garza LA, Birnbaum MJ (2000). Insulin-responsive aminopeptidase trafficking in 3T3-L1 adipocytes. J Biol Chem 275, 2560–2567.

Gonzalez E, McGraw TE (2006). Insulin signaling diverges into Akt-dependent and -independent signals to regulate the recruitment/docking and the fusion of GLUT4 vesicles to the plasma membrane. Mol Biol Cell 17, 4484–4493.

Govers R, Coster AC, James DE (2004). Insulin increases cell surface GLUT4 levels by dose dependently discharging GLUT4 into a cell surface recycling pathway. Mol Cell Biol 24, 6456–6466.

Graumann J, Hubner NC, Kim JB, Ko K, Moser M, Kumar C, Cox J, Scholer H, Mann M (2008). Stable isotope labeling by amino acids in cell culture (SILAC) and proteome quantitation of mouse embryonic stem cells to a depth of 5,111 proteins. Mol Cell Proteomics 7, 672–683.

Ibarrola N, Kalume DE, Gronborg M, Iwahori A, Pandey A (2003). A proteomic approach for quantitation of phosphorylation using stable isotope labeling in cell culture. Anal Chem 75, 6043–6049.

Imamura T, Huang J, Usui I, Satoh H, Bever J, Olefsky JM (2003). Insulin-induced GLUT4 translocation involves protein kinase C-lambda-mediated functional coupling between Rab4 and the motor protein kinesin. Mol Cell Biol 23, 4892–4900.

Isabella AJ, Horne-Badovinac S (2016). Rab10-mediated secretion synergizes with tissue movement to build a polarized basement membrane architecture for organ morphogenesis. Dev Cell 38, 47–60.

Jedrychowski MP, Gartner CA, Gygi SP, Zhou L, Herz J, Kandror KV, Pilch PF (2010). Proteomic analysis of GLUT4 storage vesicles reveals LRP1 to be an important vesicle component and target of insulin signaling. J Biol Chem 285, 104–114.

Karylowski O, Zeigerer A, Cohen A, McGraw TE (2004). GLUT4 is retained by an intracellular cycle of vesicle formation and fusion with endosomes. Mol Biol Cell 15, 870–882.

Klip A, McGraw TE, James DE (2019). Thirty sweet years of GLUT4. J Biol Chem 294, 11369–11381.

Klumperman J (2011). Architecture of the mammalian Golgi. Cold Spring Harb Perspect Biol 3.

Kristiansen S, Richter EA (2002). GLUT4-containing vesicles are released from membranes by phospholipase D cleavage of a GPI anchor. Am J Physiol Endocrinol Metab 283, E374–E382.

Lampson MA, Racz A, Cushman SW, McGraw TE (2000). Demonstration of insulin-responsive trafficking of GLUT4 and vpTR in fibroblasts. J Cell Sci 113 (Pt 22), 4065–4076.

Lampson MA, Schmoranzer J, Zeigerer A, Simon SM, McGraw TE (2001). Insulin-regulated release from the endosomal recycling compartment

is regulated by budding of specialized vesicles. Mol Biol Cell 12, 3489–3501.
Lansey MN, Walker NN, Hargett SR, Stevens JR, Keller SR (2012). Deletion of Rab GAP AS160 modifies glucose uptake and GLUT4 translocation in primary skeletal muscles and adipocytes and impairs glucose homeostasis. Am J Physiol Endocrinol Metab 303, E1273–E1286.
Lara Ordonez AJ, Fernandez B, Fdez E, Romo-Lozano M, Madero-Perez J, Lobbestael E, Baekelandt V, Aiastui A, de Munain AL, Melrose HL, *et al.* (2019). RAB8, RAB10 and RILPL1 contribute to both LRRK2 kinase-mediated centrosomal cohesion and ciliogenesis deficits. Hum Mol Genet 28, 3552–3568.
Larance M, Ramm G, Stockli J, van Dam EM, Winata S, Wasinger V, Simpson F, Graham M, Junutula JR, Guilhaus M, James DE (2005). Characterization of the role of the Rab GTPase-activating protein AS160 in insulin-regulated GLUT4 trafficking. J Biol Chem 280, 37803–37813.
Li LV, Bakirtzi K, Watson RT, Pessin JE, Kandror KV (2009). The C-terminus of GLUT4 targets the transporter to the perinuclear compartment but not to the insulin-responsive vesicles. Biochemical J 419, 105–113.
Liu Y, Xu XH, Chen Q, Wang T, Deng CY, Song BL, Du JL, Luo ZG (2013). Myosin Vb controls biogenesis of post-Golgi Rab10 carriers during axon development. Nat Commun 4, 2005.
Martin OJ, Lee A, McGraw TE (2006). GLUT4 distribution between the plasma membrane and the intracellular compartments is maintained by an insulin-modulated bipartite dynamic mechanism. J Biol Chem 281, 484–490.
Martin S, Millar CA, Lyttle CT, Meerloo T, Marsh BJ, Gould GW, James DE (2000a). Effects of insulin on intracellular GLUT4 vesicles in adipocytes: evidence for a secretory mode of regulation. J Cell Sci 113(Pt 19), 3427–3438.
Martin S, Ramm G, Lyttle CT, Meerloo T, Stoorvogel W, James DE (2000b). Biogenesis of insulin-responsive GLUT4 vesicles is independent of brefeldin A-sensitive trafficking. Traffic 1, 652–660.
Morris NJ, Ross SA, Lane WS, Moestrup SK, Petersen CM, Keller SR, Lienhard GE (1998). Sortilin is the major 110-kDa protein in GLUT4 vesicles from adipocytes. J Biol Chem 273, 3582–3587.
Olson AL, Trumbly AR, Gibson GV (2001). Insulin-mediated GLUT4 translocation is dependent on the microtubule network. J Biol Chem 276, 10706–10714.
Ong S-E, Blagoev B, Kratchmarova I, Kristensen DB, Steen H, Pandey A, Mann M (2002). Stable isotope labeling by amino acids in cell culture, SILAC, as a simple and accurate approach to expression proteomics. Mol Cell Proteom 1, 376–386.
Petris MJ, Mercer JF, Culvenor JG, Lockhart P, Gleeson PA, Camakaris J (1996). Ligand-regulated transport of the Menkes copper P-type ATPase efflux pump from the Golgi apparatus to the plasma membrane: a novel mechanism of regulated trafficking. EMBO J 15, 6084–6095.
Piper RC, Tai C, Kulesza P, Pang S, Warnock D, Baenziger J, Slot JW, Geuze HJ, Puri C, James DE (1993). GLUT-4 NH2 terminus contains a phenylalanine-based targeting motif that regulates intracellular sequestration. J Cell Biol 121, 1221–1232.
Roccisana J, Sadler JB, Bryant NJ, Gould GW (2013). Sorting of GLUT4 into its insulin-sensitive store requires the Sec1/Munc18 protein mVps45. Mol Biol Cell 24, 2389–2397.
Roland JT, Bryant DM, Datta A, Itzen A, Mostov KE, Goldenring JR (2011). Rab GTPase-Myo5B complexes control membrane recycling and epithelial polarization. Proc Natl Acad Sci USA 108, 2789–2794.
Sadacca LA, Bruno J, Wen J, Xiong W, McGraw TE (2013). Specialized sorting of GLUT4 and its recruitment to the cell surface are independently regulated by distinct Rabs. Mol Biol Cell 24, 2544–2557.
Sano H, Eguez L, Teruel MN, Fukuda M, Chuang TD, Chavez JA, Lienhard GE, McGraw TE (2007). Rab10, a target of the AS160 Rab GAP, is required for insulin-stimulated translocation of GLUT4 to the adipocyte plasma membrane. Cell Metab 5, 293–303.
Sano H, Kane S, Sano E, Miinea CP, Asara JM, Lane WS, Garner CW, Lienhard GE (2003). Insulin-stimulated phosphorylation of a Rab GTPase-activating protein regulates GLUT4 translocation. J Biol Chem 278, 14599–14602.
Semiz S, Park JG, Nicoloro SM, Furcinitti P, Zhang C, Chawla A, Leszyk J, Czech MP (2003). Conventional kinesin KIF5B mediates insulin-stimulated GLUT4 movements on microtubules. EMBO J 22, 2387–2399.
Shewan AM, van Dam EM, Martin S, Luen TB, Hong W, Bryant NJ, James DE (2003). GLUT4 recycles via a trans-Golgi network (TGN) subdomain enriched in Syntaxins 6 and 16 but not TGN38: involvement of an acidic targeting motif. Mol Biol Cell 14, 973–986.
Sprangers J, Rabouille C (2015). SEC16 in COPII coat dynamics at ER exit sites. Biochem Soc Trans 43, 97–103.
Steger M, Tonelli F, Ito G, Davies P, Trost M, Vetter M, Wachter S, Lorentzen E, Duddy G, Wilson S, *et al.* (2016). Phosphoproteomics reveals that Parkinson's disease kinase LRRK2 regulates a subset of Rab GTPases. Elife 5.
Sun Y, Chiu TT, Foley KP, Bilan PJ, Klip A (2014). Myosin Va mediates Rab8A-regulated GLUT4 vesicle exocytosis in insulin-stimulated muscle cells. Mol Biol Cell 25, 1159–1170.
Tan S, Ng Y, James DE (2011). Next-generation Akt inhibitors provide greater specificity: effects on glucose metabolism in adipocytes. Biochem J 435, 539–544.
Thyberg J, Moskalewski S (1999). Role of microtubules in the organization of the Golgi complex. Exp Cell Res 246, 263–279.
Tie HC, Ludwig A, Sandin S, Lu L (2018). The spatial separation of processing and transport functions to the interior and periphery of the Golgi stack. Elife 7.
Vazirani RP, Verma A, Sadacca LA, Buckman MS, Picatoste B, Beg M, Torsitano C, Bruno JH, Patel RT, Simonyte K, *et al.* (2016). Disruption of Adipose Rab10-Dependent Insulin Signaling Causes Hepatic Insulin Resistance. Diabetes 65, 1577–1589.
Wang D, Lou J, Ouyang C, Chen W, Liu Y, Liu X, Cao X, Wang J, Lu L (2010). Ras-related protein Rab10 facilitates TLR4 signaling by promoting replenishment of TLR4 onto the plasma membrane. Proc Natl Acad Sci USA 107, 13806–13811.
Whittle JR, Schwartz TU (2010). Structure of the Sec13-Sec16 edge element, a template for assembly of the COPII vesicle coat. J Cell Biol 190, 347–361.
Xiong W, Jordens I, Gonzalez E, McGraw TE (2010). GLUT4 is sorted to vesicles whose accumulation beneath and insertion into the plasma membrane are differentially regulated by insulin and selectively affected by insulin resistance. Mol Biol Cell 21, 1375–1386.
Xu Z, Kandror KV (2002). Translocation of small preformed vesicles is responsible for the insulin activation of glucose transport in adipose cells. Evidence from the in vitro reconstitution assay. J Biol Chem 277, 47972–47975.
Zeigerer A, Lampson MA, Karylowski O, Sabatini DD, Adesnik M, Ren M, McGraw TE (2002). GLUT4 retention in adipocytes requires two intracellular insulin-regulated transport steps. Mol Biol Cell 13, 2421–2435.
Zhang M, Chang H, Zhang Y, Yu J, Wu L, Ji W, Chen J, Liu B, Lu J, Liu Y, *et al.* (2012). Rational design of true monomeric and bright photoactivatable fluorescent proteins. Nat Methods 9, 727-729.